Article:
Gower, A.L. orcid.org/0000-0002-3229-5451 and Kristensson, G. (2021) Effective waves for random three-dimensional particulate materials. New Journal of Physics, 23. 063083. ISSN 1367-2630

https://doi.org/10.1088/1367-2630/abdfee

Effective waves for random three-dimensional particulate materials

EFFECTIVE WAVES FOR RANDOM THREE-DIMENSIONAL PARTICULATE MATERIALS

A PREPRINT

Artur L. Gower*
Department of Mechanical Engineering
University of Sheffield
Sheffield, UK
arturgower@gmail.com

Gerhard Kristensson†
Department of Electrical and Information Technology
Lund University
P.O. Box 118
SE-221 00 Lund, Sweden
gerhard.kristensson@eit.lth.se

January 13, 2021

ABSTRACT

How do you take a reliable measurement of a material whose microstructure is random? When using wave scattering, the answer is often to take an ensemble average (average over time or space). By ensemble averaging we can calculate the average scattered wave and the effective wavenumber. To date, the literature has focused on calculating the effective wavenumber for a plate filled with particles. One clear unanswered question was how to extend this approach to a material of any geometry and for any source. For example, does the effective wavenumber depend on only the microstructure, or also on the material geometry? In this work, we demonstrate that the effective wavenumbers depend on only microstructure, though beyond the long wavelength limit there are multiple effective wavenumbers for one fixed incident frequency. We show how to calculate the average wave scattered from a random particulate material of any shape, and for broad frequency ranges. As an example, we show how to calculate the average wave scattered from a sphere filled with particles.

***K*eywords** Ensemble averaging · Multiple scattering · Particulate materials · Wave scattering

1 Introduction

Under close inspection, many natural and synthetic materials are composed of small randomly distributed particles. This is why techniques to measure and predict these particle properties are important in many areas of science and engineering. Waves, either mechanical (like sound) or electromagnetic, are an excellent choice to probe particles because they can be non-invasive and energy efficient.

Sensing application. To develop non-invasive sensors we first need efficient mathematical models on how waves scatter. Particulate materials are valuable products across many industries. They are present in pharmaceuticals (powders and emulsions) and aerosols (suspension); metal and polymers powders for additive manufacturing, and many chemical and food industries[9, 1][1] (emulsions, colloids, slurry). Accurately monitoring the particles during processing (chemical, thermal, or mechanical) can enable automation and lead to optimised particle properties. Optimising particulates reduces waste and improves product quality. Currently there is no quantitative method to monitor dense particulates. The most reliable methods currently rely on light diffraction, which is only viable if the material is mostly transparent. In practice, this means the material needs to be diluted or filtered before applying these diffraction methods, which can only be done in small batches using in a controlled laboratory environment.

*Webpage: arturgower.github.io

†Webpage: www.eit.lth.se/personal/gerhard.kristensson

[1]Malvern Panalytical: www.malvernpanalytical.com/en/industries. Horiba Scientific: www.horiba.com/en_en/products/by-segment/scientific/particle-characterization/applications/.

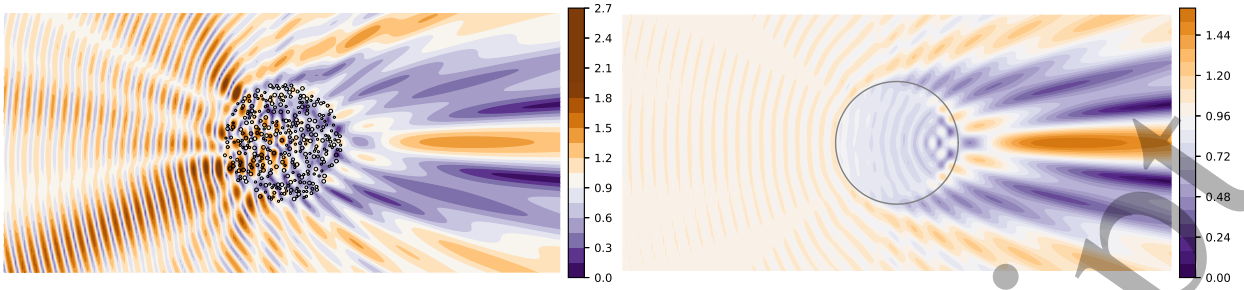

Figure 1: The figure on the left illustrates the scattered field from one configuration of particles due to an incident plane-wave [30]. The colour indicates the field value. The figure on the right illustrates the ensemble averaging of the scattered field over every possible particle configuration. Although the figure on the left shows the scattered field for one moment in time, the figure on the right is what many sensors would measure when averaging over time or space.

To develop new sensors to monitor in real time, large quantities of materials, we first need to understand how waves scatter from these dense particulates, and develop efficient models to describe this scattering.

Every particle counts. Any method that uses waves to probe a particulate material needs to consider how each particle scatters waves. This is because both particle properties and positions influence the total scattered waves, as shown in Figure 1.

Although it is possible to numerically simulate scattered waves from a specific arrangement of particles, these numerical methods are computationally too intensive for most practical applications. For example, one droplet of most emulsions will contain hundreds of millions of oil particles, whose positions are unknown. The most successful methods avoid these heavy computations by replacing the material with an equivalent homogeneous material[9, 48]. In this work we deduce this equivalent homogeneous material by taking an *ensemble average*.

The ensemble average. Ensemble averaging not only simplifies the calculations, it is also the route to devising measurements which do not depend on the positions of the particles, which are unknown. One way to do this is to take the average of the scattered field. This average can be taken over space or over time (for ergodic systems). Both of these types of average measurements eliminate the need to know the particle position, and so lead to measurements which are reproducible, even when the particle positions are unknown[20, 48].

If $u(x)$ represents the transmitted wave field, measured at some distance x, then, for a plane wave source propagating along the x-axis, it is common to approximate the ensemble average as a plane wave of the form

$$\langle u(x) \rangle \approx A \mathrm{e}^{\mathrm{i}\omega(x/c_* - t) - \alpha x}, \tag{1.1}$$

where c_* is the (effective) wave speed, α the rate of attenuation, and A the average transmission coefficient. The process of calculating the ensemble average links the measurables c_*, α, and A to the particles; it is this link which drives many sensing methods. It is common to combine c_* and α into one quantity, the complex effective wavenumber: $k_* = \omega/c_* + \mathrm{i}\alpha$. As we will see in this paper, one complicating factor is that there can be more than one transmitted wave, each with a different effective wavenumber.

What is known. One scenarios has been clearly understood: a plane wave incident on a halfspace or plate region filled with particles. This setup has, what we call in this paper, planar symmetry. For planar symmetry, in the limits of low frequency or low volume fraction, there are explicit formulas [52, 38, 45, 39, 8, 7], and an understanding on how to calculate wave reflection and transmission [44, 26]. Further, the effective wavenumbers for planar symmetry have also been rigorously deduced [25] (given typical statistical assumptions), though there is often more than one effective wavenumber for the same fixed frequency [26, 61, 62]. One clear question that remained was how to extend this approach to a material with any geometry and for any source? For example, is the effective wavenumber k_* the same for other geometries? There has even been evidence [31] that the effective properties (and wavenumber) depend on the geometry of the material. If this were true, these effective wavenumbers would not be very useful, as they would change for every sample of the same material.

In the electromagnetic community, the analysis of effective wave properties in particulate media has a long tradition. Some of the most significant contributions are collected in textbooks, *e.g.*, [56, 58, 57] and journal literature [48, 55]. With a few exceptions, the analysis deals again with planar symmetry.

This paper. Here we develop the theory for effective waves and wavenumbers for materials in any geometry. The key to achieve this is to use the representation:

$$\langle u(x,t)\rangle = \sum_{p=1}^{P} \phi_p(x)\mathrm{e}^{-\mathrm{i}\omega t}, \tag{1.2}$$

where $\phi_p(x)$ is a function that satisfies $\nabla^2\phi_p(x) + k_p^2\phi_p(x) = 0$. This representation allows us to deduce a dispersion equation for the k_p that does not depend on the material geometry. This question of whether the geometry changes the effective wavenumbers has been raised in previous studies [31].Note we will work solely in the frequency domain and therefore omit the $\mathrm{e}^{-\mathrm{i}\omega t}$ factor.

In this paper we present a framework for effective scalar waves in any material geometry, and then specialise to a material shaped as a sphere and a plate. This allows us to design highly efficient numerical methods for these cases.

2 A collection of particles

We begin with the deterministic many-particle scattering problem and use the Null-field approach [36]. Consider J different particles, where the i-th particle is centred at the location $\boldsymbol{r}_i$ as shown in Figure 2.[2] The radius of the minimum circumscribed sphere, centred at $\boldsymbol{r}_i$, is a_i, $i = 1, 2, \ldots, J$. We assume that no minimum circumscribed spheres intersect. Each particle can have a different shape and material properties.

The particles are located in a homogeneous, isotropic media with wavenumber k, which is either a real number or a complex number with a positive imaginary part.

The prescribed sources are located in the region V_{in}, which is a region disjoint to all particles,[3] and these sources generate the field $u_{\mathrm{in}}(\boldsymbol{r})$ everywhere outside V_{in}.

For a point $\boldsymbol{r}$, outside of the circumscribed spheres of all particles, we can write the total field $u(\boldsymbol{r})$ as a sum of the incident wave $u_{\mathrm{in}}(\boldsymbol{r})$ and all scattered waves in the form [33, 36, 38]

$$u(\boldsymbol{r}) = u_{\mathrm{in}}(\boldsymbol{r}) + u_{\mathrm{sc}}(\boldsymbol{r}), \quad u_{\mathrm{sc}}(\boldsymbol{r}) = \sum_{i=1}^{J}\sum_{n} f_n^i \mathrm{u}_n(k\boldsymbol{r} - k\boldsymbol{r}_i), \tag{2.1}$$

where we assumed $|\boldsymbol{r} - \boldsymbol{r}_i| > a_i$ for $i = 1, 2, \ldots J$, the f_n^i are coefficients we need to determine, and for convenience we use scalar spherical waves:

$$\begin{cases} \mathrm{u}_n(k\boldsymbol{r}) = \mathrm{h}_\ell^{(1)}(kr)\mathrm{Y}_n(\hat{\boldsymbol{r}}), & \text{(outgoing spherical waves)} \\ \mathrm{v}_n(k\boldsymbol{r}) = \mathrm{j}_\ell(kr)\mathrm{Y}_n(\hat{\boldsymbol{r}}), & \text{(regular spherical waves)} \end{cases} \tag{2.2}$$

where $r = |\boldsymbol{r}|$, and n denotes a multi index $n = \{\ell, m\}$, with summation being over $\ell = 0, 1, 2, 3\ldots$ and $m = -\ell, -\ell+1, \ldots, -1, 0, 1, \ldots, \ell$. For more details, see Appendix A. The spherical Hankel and Bessel functions are denoted $\mathrm{h}_\ell^{(1)}(z)$ and $\mathrm{j}_\ell(z)$, respectively. The field $\sum_n f_n^i \mathrm{u}_n(k\boldsymbol{r} - k\boldsymbol{r}_i)$ is the wave scattered from particle-i.

Together, $\mathrm{u}_n(k\boldsymbol{r})$ and $\mathrm{v}_n(k\boldsymbol{r})$, for all n, form a complete basis that can be used to expand solutions to wave equations. This expansion is written in terms of a series, which is guaranteed to converge in a spherical region. For details on spherical wave expansions see [50, §7.2 & §8.2] and [45]..

2.1 Incident field

We assume the incident field is generated outside of all particles, see Figure 2, so it has an expansion in regular spherical waves

$$u_{\mathrm{in}}(\boldsymbol{r}) = \sum_n g_n \mathrm{v}_n(k\boldsymbol{r}) = \sum_{nn'} g_n \mathcal{V}_{nn'}(k\boldsymbol{r}_i)\mathrm{v}_{n'}(k\boldsymbol{r} - k\boldsymbol{r}_i), \tag{2.3}$$

where for the last equality we used a translation matrix of the regular spherical waves, $\mathcal{V}_{nn'}(k\boldsymbol{r}_i)$, to write the incident wave in terms of spherical waves centred at $\boldsymbol{r}_i$. See Appendix B for details.

[2] Throughout this paper, vector-valued quantities are denoted in italic boldface and vectors of unit length have a "hat" or caret (ˆ) over the symbol.

[3] More precisely, the circumscribed sphere of the source region must not include any local origin $\boldsymbol{r}_i$, $i = 1, 2, \ldots, J$. For instance, an incident plane wave fulfils these restrictions.

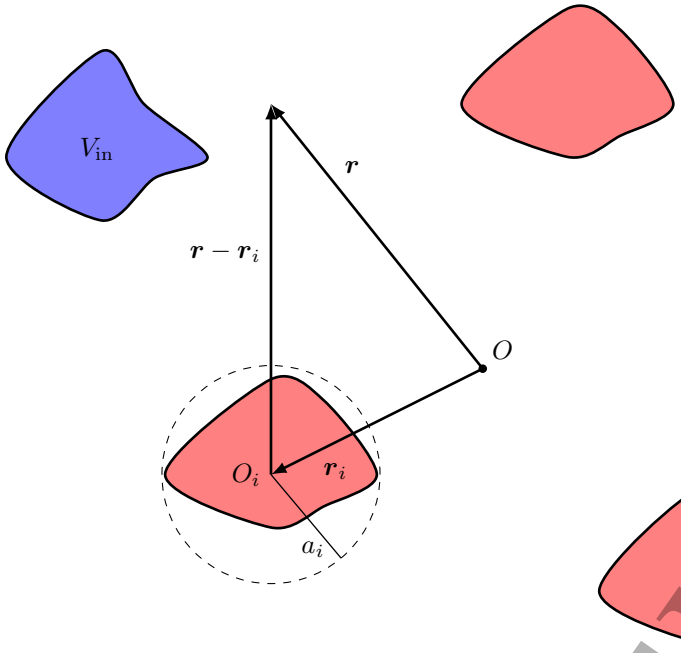

Figure 2: The geometry of a collection of the J particles and the region of prescribed sources V_{in}. The common origin is denoted O. The positions of the local origins O_i are $\boldsymbol{r}_i$, $i = 1, \ldots, J$, and the radius of the minimum circumscribed sphere of each local particle is a_i.

In many applications, we adopt a plane wave impinging along the direction $\hat{\boldsymbol{k}}$, *i.e.*,

$$u_{\text{in}}(\boldsymbol{r}) = \mathrm{e}^{\mathrm{i}k\hat{\boldsymbol{k}}\cdot\boldsymbol{r}}, \tag{2.4}$$

where the expansion coefficients, g_n, are given by [36]

$$g_n = 4\pi \mathrm{i}^{\ell} \mathrm{Y}_n^*(\hat{\boldsymbol{k}}), \tag{2.5}$$

where a star * denotes complex conjugate. For the special direction $\hat{\boldsymbol{k}} = \hat{\boldsymbol{z}}$, the coefficients are simplified

$$g_n = 4\pi \mathrm{i}^{\ell} \mathrm{Y}_n^*(\hat{\boldsymbol{z}}) = \mathrm{i}^{\ell} \delta_{m,0} \sqrt{4\pi(2\ell+1)}. \tag{2.6}$$

2.2 Scattered field

The coefficients f_n^i from (2.1) are determined by using the T-matrix to relate the field incident on the i-th particle, $u(\boldsymbol{r}) - \sum_n f_n^i \mathrm{u}_n(k\boldsymbol{r} - k\boldsymbol{r}_i)$, to the wave scattered from the i-th particle, $\sum_n f_n^i \mathrm{u}_n(k\boldsymbol{r} - k\boldsymbol{r}_i)$, which leads to [33, 36, 38]

$$f_n^i = \sum_{n'} T_n^i \mathcal{V}_{n'n}(k\boldsymbol{r}_i) g_{n'} + \sum_{\substack{j=1 \\ j\neq i}}^{J} \sum_{n'} T_n^i \mathcal{U}_{n'n}(k\boldsymbol{r}_i - k\boldsymbol{r}_j) f_{n'}^j, \quad i = 1, 2, \ldots, J, \tag{2.7}$$

where $\mathcal{U}_{nn'}$ is the translation matrix of the outgoing spherical waves u_n, see Appendix B. Above we have used a diagonal T-matrix which assumes a spherical particle; later we will explain how this leads to the solution for non-spherical particles whose orientation is independent of position and properties.

Equation (2.7) is very difficult to calculate when the number of particles J is large. Nevertheless, there are several software packages making substantial progress, *e.g.*, MSTM (Multiple Sphere T Matrix) [43, 22, 23].

The T_n^i depend only on the properties of the i-th particle, while the scattering coefficients f_n^i depends on the positions and properties of all the particles. For example, for acoustics, and a homogeneous spherical particle, we would have [38]:

$$T_n^i = -\frac{\gamma_i \mathrm{j}_\ell'(ka_i)\mathrm{j}_\ell(k_i a_i) - \mathrm{j}_\ell(ka_i)\mathrm{j}_\ell'(k_i a_i)}{\gamma_i \mathrm{h}_\ell^{(1)\prime}(ka_i)\mathrm{j}_\ell(k_i a_i) - \mathrm{h}_\ell^{(1)}(ka_i)\mathrm{j}_\ell'(k_i a_i)}, \tag{2.8}$$

where $\gamma_i = \rho_i k/(\rho k_i)$, a_i is the particle radius, ρ is the background density, while ρ_i and k_i are the density and wavenumber of the particle.

3 Ensemble averaging

Even if the position and properties of all particles were known, it is still very challenging to solve (2.7) for a large number of particles, say, over 10^6. Also, many sensors can not even measure f_n^i, but instead measure the scattered field averaged either in time or space. For many systems, this average over time or space is equivalent to an ensemble average [20, 48], which we describe below and can be used to calculate the average of the scattered waves. The first step towards achieving this is to introduce a probability for the particles having certain properties and positions [38, 33, 56, 55].

3.1 Statistical assumptions

To describe the properties and shape of the i-th particle, we will use the variable λ_i, which allows us to define $T_n(\lambda_i) := T_n^i$ for every i. This means that the f_n^i, governed by (2.7), depend on the positions $\boldsymbol{r}_1, \boldsymbol{r}_2, \ldots, \boldsymbol{r}_J$ and the properties $\lambda_1, \lambda_2, \ldots, \lambda_J$ of all the particles.

To ensemble average we need to assign a probability density for any configuration $\boldsymbol{r}_1, \boldsymbol{r}_2, \ldots, \boldsymbol{r}_J$, and any properties $\lambda_1, \lambda_2, \ldots, \lambda_J$. The first step is to consider the $\boldsymbol{r}_i$ and λ_i as random variables. Next we assume that the particle properties λ_i are sampled from the same domain $\mathcal{S}$. For example, if $\lambda_i = a_i$, the radius of particle-i, for every i, then we could choose $\mathcal{S} = [A_1, A_2]$ so that all $\lambda_i \in \mathcal{S}$, *i.e.*, we restrict all particle radii in some interval. For particle origins $\boldsymbol{r}_i$ we can not restrict them all to the same domain because the particles may have a different sizes. So instead we choose a different domain for each, that is, for a given λ_i we have that $r_i \in \mathcal{R}_i$. For example, if all the particles were contained in a sphere with of radius R, then a particle with radius a_i would have its origin $\boldsymbol{r}_i$ restricted in a sphere of radius $R - a_i$. That is, $\mathcal{R}_i$ would be a sphere of radius $R - a_i$.

The main parameters we use to describe the average particulate material are

$$\mathfrak{n}(\lambda_i) = \frac{J}{|\mathcal{R}_i|} p(\lambda_i) \quad \text{(number of } \lambda_i \text{ types particles per unit volume)}, \tag{3.1}$$

$$a_{ij} \quad \text{(the minimal allowed distance } |\boldsymbol{r}_i - \boldsymbol{r}_j| \text{ between particle } i \text{ and particle } j), \tag{3.2}$$

where $|\mathcal{R}_i|$ is the volume of $\mathcal{R}_i$ and $p(\lambda_i)$ is the probability density of the particle having the property λ_i. In this paper we allow the minimal distance between two particles a_{ij} to be larger or equal to the sum of the particle radii $a_i + a_j$. Note we committed an abuse of notation for the function p, and will continue to do so.

Let $p(\boldsymbol{r}_i, \lambda_i)$ be the probability density of having a particle centred at $\boldsymbol{r}_i \in \mathcal{R}_i$ with $\lambda_i \in \mathcal{S}$, after ensemble averaging over all other particle positions and properties. If we assume that $\boldsymbol{r}_i$ is equally likely to be anywhere in $\mathcal{R}_i$ we obtain

$$p(\boldsymbol{r}_i, \lambda_i) = p(\boldsymbol{r}_i|\lambda_i)p(\lambda_i) \approx \frac{p(\lambda_i)}{|\mathcal{R}_i|} = \frac{\mathfrak{n}(\lambda_i)}{J}. \tag{3.3}$$

We also need to define conditional probabilities:

$$p(\boldsymbol{r}_1, \lambda_1; \ldots; \boldsymbol{r}_{i-1}, \lambda_{i-1}; \boldsymbol{r}_{i+1}, \lambda_{i+1}; \ldots; \boldsymbol{r}_M, \lambda_M | \boldsymbol{r}_i, \lambda_i) = p(\boldsymbol{r}_1, \lambda_1; \ldots; \boldsymbol{r}_M, \lambda_M)/p(\boldsymbol{r}_i, \lambda_i), \tag{3.4}$$

where M is any integer smaller than the number of particles J.

To solve the ensemble average equations, the probability function for two particles $p(\boldsymbol{r}_i, \lambda_i; \boldsymbol{r}_j, \lambda_j)$ needs to be given. To achieve this, we use an assumption called *hole correction*, which assumes that any two particles are equally likely to be anywhere within regions[4], except that their minimum circumscribed spheres do not overlap [18, 19]:

$$p(\boldsymbol{r}_i; \boldsymbol{r}_j|\lambda_i; \lambda_j) \approx \begin{cases} \frac{1}{|\mathcal{R}_i||\mathcal{R}_j|} & \text{for } |\boldsymbol{r}_i - \boldsymbol{r}_j| \geq a_{ij}, \\ 0 & \text{for } |\boldsymbol{r}_i - \boldsymbol{r}_j| < a_{ij}. \end{cases} \tag{3.5}$$

To deduce the above for $|\boldsymbol{r}_i - \boldsymbol{r}_j| \geq a_{ij}$ we used

$$p(\boldsymbol{r}_i; \boldsymbol{r}_j|\lambda_i; \lambda_j) = p(\boldsymbol{r}_i|\lambda_i; \lambda_j)p(\boldsymbol{r}_j|\boldsymbol{r}_i, \lambda_i; \lambda_j) \approx \frac{1}{|\mathcal{R}_i|}\frac{1}{|\mathcal{R}_j|}, \tag{3.6}$$

[4]When $\boldsymbol{r}_i$ or $\boldsymbol{r}_j$ are very close to the boundary of their regions $\mathcal{R}_i$ and $\mathcal{R}_j$, then (3.5) should be altered. We do not include this alteration because it does not affect any of the results on effective waves.

where $p(\boldsymbol{r}_i;\boldsymbol{r}_j|\lambda_i;\lambda_j)$ is the probability density of having one particle centred at $\boldsymbol{r}_i$, knowing that it has the property λ_i, and another particle at $\boldsymbol{r}_j$, knowing that it has the property λ_j. The approximation above assumes that the volume of one particle is negligible in comparison to the volume of its confining region.

To help interpret hole-correction (3.5) we will do some extra calculations. For simplicity, we assume that the particle properties λ_i and λ_j are independent of each other to reach

$$p(\boldsymbol{r}_j,\lambda_j|\boldsymbol{r}_i,\lambda_i)=\frac{p(\boldsymbol{r}_i,\lambda_i;\boldsymbol{r}_j,\lambda_j)}{p(\boldsymbol{r}_i,\lambda_i)}\approx|\mathcal{R}_i|p(\lambda_j)p(\boldsymbol{r}_i;\boldsymbol{r}_j|\lambda_i;\lambda_j)\approx\begin{cases}\frac{\mathfrak{n}(\lambda_j)}{J} & \text{for } |\boldsymbol{r}_i-\boldsymbol{r}_j|\geq a_{ij},\\ 0 & \text{for } |\boldsymbol{r}_i-\boldsymbol{r}_j|<a_{ij},\end{cases}\tag{3.7}$$

where for the last approximation we used (3.5) and (3.1). An alternative way to calculate the above is to approximate $p(\boldsymbol{r}_j,\lambda_j|\boldsymbol{r}_i,\lambda_i)$ for its expected value in $\boldsymbol{r}_i$ and λ_i when $|\boldsymbol{r}_i-\boldsymbol{r}_j|\geq a_{ij}$, that is

$$p(\boldsymbol{r}_j,\lambda_j|\boldsymbol{r}_i,\lambda_i)\approx\int_{\mathcal{R}_i}\int_{\mathcal{S}}p(\boldsymbol{r}_i,\lambda_i)p(\boldsymbol{r}_j,\lambda_j|\boldsymbol{r}_i,\lambda_i)\mathrm{d}\boldsymbol{r}_i\mathrm{d}\lambda_i=p(\boldsymbol{r}_j,\lambda_j),\quad\text{for }|\boldsymbol{r}_i-\boldsymbol{r}_j|\geq a_{ij},\tag{3.8}$$

which when using (3.3) leads to the same conclusion as hole correction (3.7). Here, $\mathrm{d}\boldsymbol{r}_i$ is the volume measure of the region $\mathcal{R}_i$. Later, we show that the quasi-crystalline approximation (3.12) makes an approximation which is analogous to (3.8).

We can now define the ensemble average of f_n^1 as

$$\langle f_n^1\rangle=\int f_n^1\,p(\boldsymbol{r}_1,\lambda_1;\ldots;\boldsymbol{r}_J,\lambda_J)\mathrm{d}\boldsymbol{r}_1\cdots\mathrm{d}\boldsymbol{r}_J\mathrm{d}\lambda_1\cdots\mathrm{d}\lambda_J,\tag{3.9}$$

where the above integrals are over all feasible values for the particles positions $\boldsymbol{r}_i$ and properties λ_i.

We also need the conditional ensemble averages, which we define as

$$\langle f_n^1\rangle(\boldsymbol{r}_1,\lambda_1)=\int f_n^1\,p(\boldsymbol{r}_2,\lambda_2;\ldots;\boldsymbol{r}_J,\lambda_J|\boldsymbol{r}_1,\lambda_1)\mathrm{d}\boldsymbol{r}_2\cdots\mathrm{d}\boldsymbol{r}_J\mathrm{d}\lambda_2\cdots\mathrm{d}\lambda_J,\tag{3.10}$$

$$\langle f_n^2\rangle(\boldsymbol{r}_1,\lambda_1;\boldsymbol{r}_2,\lambda_2)=\int f_n^2\,p(\boldsymbol{r}_3,\lambda_3;\ldots;\boldsymbol{r}_J,\lambda_J|\boldsymbol{r}_1,\lambda_1;\boldsymbol{r}_2,\lambda_2)\mathrm{d}\boldsymbol{r}_3\cdots\mathrm{d}\boldsymbol{r}_J\mathrm{d}\lambda_3\cdots\mathrm{d}\lambda_J.\tag{3.11}$$

Note that in (3.10) we are holding the first particle's position $\boldsymbol{r}_1$ and properties λ_1 fixed while averaging over the other particles. In (3.11) we are averaging f_n^2 while holding the first and second particles positions $\boldsymbol{r}_1$, $\boldsymbol{r}_2$ and properties λ_1, λ_2 fixed.

For consistency and simplicity, we will use an approximation for $\langle f_n^2\rangle(\boldsymbol{r}_1,\lambda_1;\boldsymbol{r}_2,\lambda_2)$ which is analogous to both (3.8) and (3.5), and is called the quasi-crystalline approximation:

$$\langle f_n^2\rangle(\boldsymbol{r}_1,\lambda_1;\boldsymbol{r}_2,\lambda_2)\approx\langle f_n^2\rangle(\boldsymbol{r}_2,\lambda_2),\quad\text{for }|\boldsymbol{r}_1-\boldsymbol{r}_2|>a_{12}.\tag{3.12}$$

That is, we replace $\langle f_n^2\rangle(\boldsymbol{r}_1,\lambda_1;\boldsymbol{r}_2,\lambda_2)$ for its expected value in $\boldsymbol{r}_1$ and λ_1, see [28] for a brief discussion on the topic. This is a standard approach used across statistical physics. It is called a closure approximation [37, 2].

Because the particles only differ due to their position $\boldsymbol{r}_i$ and properties λ_i, we have that $\langle f_n^i\rangle(\boldsymbol{r}_i,\lambda_i)=\langle f_n^j\rangle(\boldsymbol{r}_j,\lambda_j)$ for any i and j. That is, all particles with the same properties are indistinguishable. This is why we now define:

$$\langle f_n\rangle(\boldsymbol{r}_j,\lambda_j):=\langle f_n^j\rangle(\boldsymbol{r}_j,\lambda_j)\quad\text{for }j=1,2,\ldots,J.\tag{3.13}$$

3.2 Average scattered field

To calculate the ensemble average scattered field we first choose a point $\boldsymbol{r}$ outside of the material, where we want to measure the scattered field. For example, turning to Figure 3, the point $\boldsymbol{r}$ needs to be outside of $\mathcal{R}_2$ and at least one particle radius a_2 away from the boundary of $\mathcal{R}_2$. Then we multiply both sides of (2.1) by $p(\boldsymbol{r}_1,\ldots,\boldsymbol{r}_J,\lambda_1,\ldots,\lambda_J)$ and integrate over all possible particle positions and properties to reach

$$\langle u(\boldsymbol{r})\rangle=u_{\mathrm{in}}(\boldsymbol{r})+\langle u_{\mathrm{sc}}(\boldsymbol{r})\rangle,\tag{3.14}$$

where $\langle u_{\mathrm{in}}(\boldsymbol{r})\rangle=u_{\mathrm{in}}(\boldsymbol{r})$, because the incident wave does not depend on the particle configuration, and

$$\begin{aligned}\langle u_{\mathrm{sc}}(\boldsymbol{r})\rangle&=J\sum_n\int_{\mathcal{S}}\int_{\mathcal{R}_1}\langle f_n\rangle(\boldsymbol{r}_1,\lambda_1)\mathrm{u}_n(k\boldsymbol{r}-k\boldsymbol{r}_1)p(\boldsymbol{r}_1,\lambda_1)\mathrm{d}\boldsymbol{r}_1\mathrm{d}\lambda_1\\&\approx\sum_n\int_{\mathcal{S}}\mathfrak{n}(\lambda_1)\int_{\mathcal{R}_1}\langle f_n\rangle(\boldsymbol{r}_1,\lambda_1)\mathrm{u}_n(k\boldsymbol{r}-k\boldsymbol{r}_1)\mathrm{d}\boldsymbol{r}_1\mathrm{d}\lambda_1,\end{aligned}\tag{3.15}$$

where we used (3.3), (3.4), and (3.13). Note that to take the limit $J \to \infty$, it normally makes sense to fix the number density $\mathfrak{n}(\lambda_i)$ and the probability $p(\lambda_i)$, and then allow the volume of the region $|\mathcal{R}_i|$ to grow with J.

We can rewrite the above when $|\boldsymbol{r}| > |\boldsymbol{r}_1|$ for every $\boldsymbol{r}_1 \in \mathcal{R}_1$. In this case, we can use the translation matrix (B.1) for u_n to obtain

$$\langle u_{\mathrm{sc}}(\boldsymbol{r})\rangle = \sum_n \mathfrak{F}_n \mathrm{u}_n(k\boldsymbol{r}), \quad \text{with} \quad \mathfrak{F}_n = \sum_{n'} \int_{\mathcal{S}} \mathfrak{n}(\lambda_1) \int_{\mathcal{R}_1} \mathcal{V}_{n'n}(-k\boldsymbol{r}_1)\langle f_{n'}\rangle(\boldsymbol{r}_1,\lambda_1)\, \mathrm{d}\boldsymbol{r}_1\, \mathrm{d}\lambda_1. \tag{3.16}$$

The $\mathfrak{F}_n$ are then the average scattering coefficients of the whole material.

3.3 Average governing equations

To calculate $\langle f_n\rangle(\boldsymbol{r}_1,\lambda_1)$, we need to ensemble average the governing equation (2.7). To achieve this, we set $i = 1$, multiply both sides of (2.7) by $p(\boldsymbol{r}_2,\lambda_2;\boldsymbol{r}_3,\lambda_3;\ldots;\boldsymbol{r}_J,\lambda_J|\boldsymbol{r}_1,\lambda_1)$, and then integrate over all feasible positions and properties while holding $\boldsymbol{r}_1$ and λ_1 fixed. Then, to transform the result into an equation where $\langle f_n(\boldsymbol{r}_1,\lambda_1)\rangle$ is the only unknown we use (3.7) and (3.12), to obtain

$$\begin{aligned}\langle f_n\rangle(\boldsymbol{r}_1,\lambda_1) &= T_n(\lambda_1)\sum_{n'} \mathcal{V}_{n'n}(k\boldsymbol{r}_1) g_{n'} \\ &+ T_n(\lambda_1)\sum_{n'}\int_{\mathcal{S}} \bar{\mathfrak{n}}(\lambda_2)\int_{\mathcal{R}_2\setminus\mathcal{B}(\boldsymbol{r}_1;a_{12})} \mathcal{U}_{n'n}(k\boldsymbol{r}_1 - k\boldsymbol{r}_2)\langle f_{n'}\rangle(\boldsymbol{r}_2,\lambda_2)\mathrm{d}\boldsymbol{r}_2\mathrm{d}\lambda_2,\end{aligned} \tag{3.17}$$

for all $\boldsymbol{r}_1 \in \mathcal{R}_1$ and $\lambda_1 \in \mathcal{S}$, where we define

$$\mathcal{B}(\boldsymbol{r}_1;R) = \{\boldsymbol{r} : |\boldsymbol{r}-\boldsymbol{r}_1| \le R\}, \tag{3.18}$$

used $\mathcal{R}_2 \setminus \mathcal{B}(\boldsymbol{r}_1;a_{12}) = \{\boldsymbol{r} \in \mathcal{R}_2 : \boldsymbol{r} \notin \mathcal{B}(\boldsymbol{r}_1;a_{12})\}$ and $\bar{\mathfrak{n}}(\lambda_2) = \frac{J-1}{J}\mathfrak{n}(\lambda_2)$.

The system (3.17) can be used to solve for $f_n(\boldsymbol{r}_1,\lambda_1)$ for any given material geometry $\mathcal{R}_1$ and any T-matrix T_n. If all particles were the same, *i.e.*, same shape and properties, then (3.17) would be equivalent to [38, Equation (4.13)] and [33, Equation (12)]. If we considered a two dimensional material, with different types of particles, then (3.17) would be equivalent to [28, Equation (3.6)].

1. Averaging non-spherical particles

As an aside, we explain how (3.17) can accommodate particles which are not exactly spherical, as shown in Figure 2.

Assume we have non-spherical particles with a T-matrix $T_{nn'}(\lambda_j,\tau_j)$, which depends on the particle properties λ_j and orientation τ_j. If every particle's orientation is statistically independent from everything else[a], then we can set the T_n in (3.17) to equal

$$T_n(\lambda_j) = \int T_{nn}(\lambda_j,\tau_j)p(\tau_j)\mathrm{d}\tau_j,$$

where $p(\tau_j)$ is the probability density of particle j being rotated by a τ_j angle. Note that in general τ_j could represent three Euler angles. In particular, if the particle is equally likely to be oriented in any direction then the $T_{nn'}(\lambda_j,\tau_j)$ averaged over every angle τ_j becomes diagonal [47, 59].

[a] Including the minimal allowed distance between any two particles (3.2).

3.4 Symmetry reductions

Before solving (3.17) to determine the field $\langle f_n\rangle(\boldsymbol{r}_1,\lambda_1)$, we first look at how to use symmetries to represent $\langle f_n\rangle(\boldsymbol{r}_1,\lambda_1)$ in a reduced form.

We could apply symmetry reduction directly to the governing integral equation (3.17). It is, however, simpler to just impose symmetries on the average scattered wave $\langle u_{\mathrm{sc}}(\boldsymbol{r})\rangle$ (3.15) and then deduce the resulting symmetry for $\langle f_n\rangle(\boldsymbol{r}_1,\lambda_1)$ as we demonstrate below. To omit a heavy notation, we will in this section omit the dependence of $\langle f_n\rangle$ on λ_1 and the integrals over the particles properties $\mathcal{S}$.

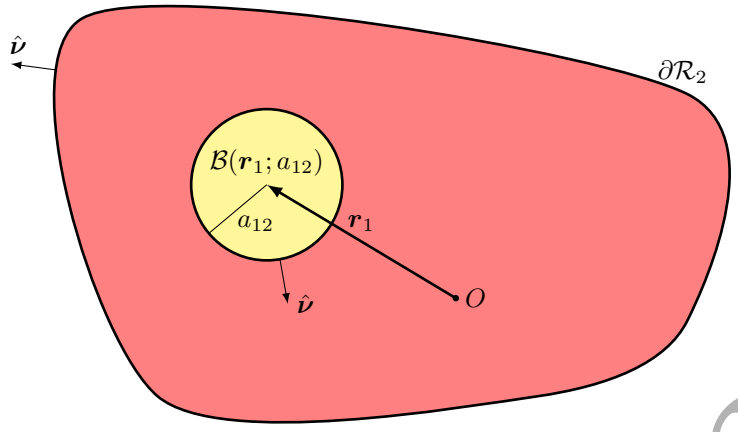

Figure 3: The geometry of the region $\mathcal{R}_2$ (red) and the hole correction $\mathcal{B}(\boldsymbol{r}_1; a_{12})$ (in yellow) centred at $\boldsymbol{r}_1$. The figure also displays the direction of the surface unit vectors $\hat{\boldsymbol{\nu}}$.

Azimuthal symmetry: we expect this symmetry when the total scattered wave $u_{\rm sc}$ does not change when rotating the measurement point $\boldsymbol{r}$ around the $z-$axis. This occurs, for example, for the incident plane wave $u_{\rm in}(\boldsymbol{r}) = \mathrm{e}^{\mathrm{i}kz}$ and a spherical material region $\mathcal{R}_1 = \{|\boldsymbol{r}| \leq R : \boldsymbol{r} \in \mathbb{R}^3\}$ centred at the origin. When azimuthal symmetry is present, we expect

$$\langle u_{\rm sc}(\mathbf{P}\boldsymbol{r})\rangle = \langle u_{\rm sc}(\boldsymbol{r})\rangle \quad \text{for every } |\boldsymbol{r}| \notin \mathcal{R}_1,$$

where we define the operator $\mathbf{P}$ such that $\mathbf{P}\boldsymbol{r}$ is a ϕ_0 rotation of the vector $\boldsymbol{r}$ around the z-axis. Note that when $\mathcal{R}_1$ is a sphere, then the above should hold true for $\boldsymbol{r} \geq R$.

To determine the consequences of this symmetry, we turn to the average scattered wave (3.15) and rewrite in the form

$$\begin{aligned}\langle u_{\rm sc}(\mathbf{P}\boldsymbol{r})\rangle &= \sum_n \int_{\mathcal{R}_1} \langle f_n\rangle(\boldsymbol{r}_1)\mathrm{u}_n(k\mathbf{P}\boldsymbol{r} - k\boldsymbol{r}_1)\mathrm{d}\boldsymbol{r}_1 = \sum_n \int_{\mathcal{R}_1} \langle f_n\rangle(\mathbf{P}\boldsymbol{r}_1)\mathrm{u}_n(k\mathbf{P}\boldsymbol{r} - k\mathbf{P}\boldsymbol{r}_1)\mathrm{d}\boldsymbol{r}_1 \\ &= \sum_n \int_{\mathcal{R}_1} \langle f_n\rangle(\mathbf{P}\boldsymbol{r}_1)\mathrm{e}^{\mathrm{i}m\phi_0}\mathrm{u}_n(k\boldsymbol{r} - k\boldsymbol{r}_1)\mathrm{d}\boldsymbol{r}_1,\end{aligned}$$

where we used a change of variables $\boldsymbol{r}_1 \to \mathbf{P}\boldsymbol{r}_1$, and used (2.2) and (A.1) to substitute $\mathrm{u}_n(k\mathbf{P}\boldsymbol{r} - k\mathbf{P}\boldsymbol{r}_1) = \mathrm{e}^{\mathrm{i}m\phi_0}\mathrm{u}_n(k\boldsymbol{r} - k\boldsymbol{r}_1)$. Notice that the volume measure $\mathrm{d}\mathbf{P}\boldsymbol{r}_1 = \mathrm{d}\boldsymbol{r}_1$. Equating the above to $\langle u_{\rm sc}(\boldsymbol{r})\rangle$ and using (3.15) then suggests that $\langle f_n\rangle(\boldsymbol{r}_1) = \langle f_n\rangle(\mathbf{P}\boldsymbol{r}_1)\mathrm{e}^{\mathrm{i}m\phi_0}$. Then by using a spherical coordinate system (r_1, θ_1, ϕ_1) for $\boldsymbol{r}_1$, and by choosing $\phi_0 = -\phi_1$ (without loss of generality) we find that (arguments in spherical coordinates)

$$\langle f_n\rangle(r_1, \theta_1, \phi_1) = \langle f_n\rangle(r_1, \theta_1, 0)\mathrm{e}^{-\mathrm{i}m\phi_1}, \tag{3.19}$$

for every ϕ_1. This symmetry can now be verified by checking that the right hand-side is a solution to (3.17), though this is a longer calculation.

Planar symmetry: For an incident plane wave $u_{\rm in}(\boldsymbol{r}) = \mathrm{e}^{\mathrm{i}\boldsymbol{k}\cdot\boldsymbol{r}}$ and the material region $\mathcal{R}_1 = \{\boldsymbol{r} \in \mathbb{R}^3 : z > 0\}$, we expect the average scattered wave to satisfy the planar symmetry:

$$\langle u_{\rm sc}(\boldsymbol{r})\rangle = \langle u_{\rm sc}(\boldsymbol{r} - \boldsymbol{r}_0)\rangle\mathrm{e}^{\mathrm{i}\boldsymbol{k}\cdot\boldsymbol{r}_0} \quad \text{for every } x, x_0, y, y_0 \in \mathbb{R} \text{ and } z < 0, \tag{3.20}$$

where $\boldsymbol{r}_0 = x_0\hat{\boldsymbol{x}} + y_0\hat{\boldsymbol{y}}$. If we then use (3.15) in the above we find that

$$\begin{aligned}\langle u_{\rm sc}(\boldsymbol{r} - \boldsymbol{r}_0)\rangle\mathrm{e}^{\mathrm{i}k\hat{\boldsymbol{k}}\cdot\boldsymbol{r}_0} &= \sum_n \int_{\mathcal{R}_1} \langle f_n\rangle(\boldsymbol{r}_1)\mathrm{e}^{\mathrm{i}k\hat{\boldsymbol{k}}\cdot\boldsymbol{r}_0}\mathrm{u}_n(k\boldsymbol{r} - k\boldsymbol{r}_0 - k\boldsymbol{r}_1)\ \mathrm{d}\boldsymbol{r}_1 \\ &= \sum_n \int_{\mathcal{R}_1} \langle f_n\rangle(\boldsymbol{r}_1 - \boldsymbol{r}_0)\mathrm{e}^{\mathrm{i}k\hat{\boldsymbol{k}}\cdot\boldsymbol{r}_0}\mathrm{u}_n(k\boldsymbol{r} - k\boldsymbol{r}_1)\ \mathrm{d}\boldsymbol{r}_1,\end{aligned}$$

where for the second equation we changed to the variable of integration $x_1 + x_0 \to x_1$ and $y_1 + y_0 \to y_1$. For the above to be equal to

$$\langle u_{\rm sc}(\boldsymbol{r})\rangle = \sum_n \int_{\mathcal{R}_1} \langle f_n\rangle(\boldsymbol{r}_1)\mathrm{u}_n(k\boldsymbol{r} - k\boldsymbol{r}_1)\ \mathrm{d}\boldsymbol{r}_1,$$

for every x, x_0, y, y_0, and $z<0$ suggests that $\langle f_n\rangle(\boldsymbol{r}_1)=\langle f_n\rangle(\boldsymbol{r}_1-\boldsymbol{r}_0)\mathrm{e}^{\mathrm{i}k\hat{\boldsymbol{k}}\cdot\boldsymbol{r}_0}$, then by choosing $\boldsymbol{r}_0=x_1\hat{\boldsymbol{x}}+y_1\hat{\boldsymbol{y}}$, we find that

$$\langle f_n\rangle(\boldsymbol{r}_1)=\langle f_n\rangle(z_1\hat{\boldsymbol{z}})\mathrm{e}^{\mathrm{i}k\hat{\boldsymbol{k}}\cdot(x_1\hat{\boldsymbol{x}}+y_1\hat{\boldsymbol{y}})}. \tag{3.21}$$

This symmetry can be verified by checking that the right hand-side is a solution to (3.17).

One case that combines both azimuthal (3.19) and planar symmetry (3.21) is the incident plane-wave $\mathrm{e}^{\mathrm{i}kz}$ ($\hat{\boldsymbol{k}}=\hat{\boldsymbol{z}}$) and material region $z>0$. In this case (arguments in spherical coordinates),

$$\langle f_n\rangle(r_1,\theta_1,\phi_1)=\langle f_n\rangle(r_1,0,\phi_0)=\langle f_n\rangle(r_1,0,0)\mathrm{e}^{-\mathrm{i}m\phi_0},\quad \text{for every } 0\le\phi_0\le 2\pi, \tag{3.22}$$

where the first equation is due to planar symmetry (3.21) and the second is due to azimuthal symmetry (3.19). Equation (3.22) can only be true for every ϕ_0 when

$$\langle f_n\rangle(\boldsymbol{r}_1)=\delta_{m,0}\langle f_\ell\rangle(z_1\hat{\boldsymbol{z}}).$$

This result will be used later to reach a simplified dispersion equation.

4 Effective wavenumbers

4.1 Wave decomposition

Much of the literature has focused on solving (3.17) by assuming that the unknown field $f_n(\boldsymbol{r}_1,\lambda_1)$ satisfies a wave equation for the spatial variable $\boldsymbol{r}_1$ and for some effective wavenumber k_*. This assumption implies that the average transmitted fields $\langle u(\boldsymbol{r})\rangle$ also satisfy a wave equation [44]. Recent results [26, 25] have demonstrated that for a half-space, the exact solution for $f_n(\boldsymbol{r}_1,\lambda_1)$ is a sum of plane waves, each with a different wavenumber. Here we generalise this result by considering $f_n(\boldsymbol{r}_1,\lambda_1)$ to be a sum of isotropic waves of any type, *i.e.*, not necessarily a plane wave, and the particulate material to occupy any region.

In general, we propose the representation

$$\langle f_n\rangle(\boldsymbol{r}_1,\lambda_1)=\sum_p f_{p,n}(\boldsymbol{r}_1,\lambda_1)\quad\text{with}\quad \nabla^2_{\boldsymbol{r}_1}f_{p,n}(\boldsymbol{r}_1,\lambda_1)=-k_p^2 f_{p,n}(\boldsymbol{r}_1,\lambda_1),\quad \text{for } \boldsymbol{r}_1\in\mathcal{R}_1, \tag{4.1}$$

where the Laplacian $\nabla^2_{\boldsymbol{r}_j}$ is taken in terms of $\boldsymbol{r}_j$.

Our first major result is to calculate the effective wavenumbers $k_1, k_2, \cdots$, and to demonstrate that they depend only on the particle properties, and not on the geometry of the region enclosing the particles. Although the geometry of material and the incident wave will determine which of these wavenumbers are excited. Another major result, is that most of the effective wavenumbers are highly attenuating, which implies that the series (4.1) rapidly converges to the exact solution. In the remainder of this section, we show how to deduce a system that determines the $f_{p,n}(\boldsymbol{r}_1,\lambda_1)$ that is decoupled from the material geometry.

To simplify the governing system (3.17) we note that by definition (B.1) the translation matrix $\mathcal{U}_{n'n}(k\boldsymbol{r}_1-k\boldsymbol{r}_2)$ satisfies a wave equation in either $\boldsymbol{r}_1$ or $\boldsymbol{r}_2$ with wavenumber k. This and the representation (4.1) leads to

$$\begin{aligned}(k^2-k_p^2)&\mathcal{U}_{n'n}(k\boldsymbol{r}_1-k\boldsymbol{r}_2)f_{p,n'}(\boldsymbol{r}_2,\lambda_2)\\ &=\mathcal{U}_{n'n}(k\boldsymbol{r}_1-k\boldsymbol{r}_2)\nabla^2_{\boldsymbol{r}_2}f_{p,n'}(\boldsymbol{r}_2,\lambda_2)-\nabla^2_{\boldsymbol{r}_2}\mathcal{U}_{n'n}(k\boldsymbol{r}_1-k\boldsymbol{r}_2)f_{p,n'}(\boldsymbol{r}_2,\lambda_2),\quad \text{for } \boldsymbol{r}_1\in\mathcal{R}_1.\end{aligned} \tag{4.2}$$

Then for $\boldsymbol{r}_1\in\mathcal{R}_1(a_{12})=\{\boldsymbol{r}\in\mathcal{R}_1 : d(\boldsymbol{r},\partial\mathcal{R}_1)\ge a_{12}\}$, we can integrate both sides over $\boldsymbol{r}_2\in\mathcal{R}_2\setminus\mathcal{B}(\boldsymbol{r}_1;a_{12})$ and apply Green's second identity to reach,

$$\int_{\mathcal{R}_2\setminus\mathcal{B}(\boldsymbol{r}_1;a_{12})}\mathcal{U}_{n'n}(k\boldsymbol{r}_1-k\boldsymbol{r}_2)f_{p,n'}(\boldsymbol{r}_2,\lambda_2)\mathrm{d}\boldsymbol{r}_2=\frac{\mathcal{I}_{p,n'n}(\boldsymbol{r}_1)-\mathcal{J}_{p,n'n}(\boldsymbol{r}_1)}{k^2-k_p^2},\quad \boldsymbol{r}_1\in\mathcal{R}_2(a_{12}) \tag{4.3}$$

where

$$\mathcal{I}_{p,n'n}(\boldsymbol{r}_1)=\int_{\partial\mathcal{R}_2}\mathcal{U}_{n'n}(k\boldsymbol{r}_1-k\boldsymbol{r}_2)\frac{\partial f_{p,n'}(\boldsymbol{r}_2,\lambda_2)}{\partial\boldsymbol{\nu}_2}-\frac{\partial\mathcal{U}_{n'n}(k\boldsymbol{r}_1-k\boldsymbol{r}_2)}{\partial\boldsymbol{\nu}_2}f_{p,n'}(\boldsymbol{r}_2,\lambda_2)\mathrm{d}A_2, \tag{4.4}$$

$$\mathcal{J}_{p,n'n}(\boldsymbol{r}_1)=\int_{\partial B(\boldsymbol{0};a_{12})}\mathcal{U}_{n'n}(-k\boldsymbol{r})\frac{\partial f_{p,n'}(\boldsymbol{r}+\boldsymbol{r}_1,\lambda_2)}{\partial\boldsymbol{\nu}}-\frac{\partial\mathcal{U}_{n'n}(-k\boldsymbol{r})}{\partial\boldsymbol{\nu}}f_{p,n'}(\boldsymbol{r}+\boldsymbol{r}_1,\lambda_2)\mathrm{d}A, \tag{4.5}$$

$\mathrm{d}A_2$ and $\mathrm{d}A$ are the surface elements for $\boldsymbol{r}_2$ and $\boldsymbol{r}$, respectively, and $\boldsymbol{\nu}_2$ and $\boldsymbol{\nu}$ are outward pointing normal vectors to the surfaces $\partial\mathcal{R}_2$ and $\partial B(\boldsymbol{0};a_{12})$, respectively (see Figure 3). To reach (4.5) we changed the integration variable to $\boldsymbol{r}=\boldsymbol{r}_2-\boldsymbol{r}_1$.

Both integrals $\mathcal{I}_{p,n'n}(\boldsymbol{r}_1)$ and $\mathcal{J}_{p,n'n}(\boldsymbol{r}_1)$ depend on the state variable λ_1 and λ_2, which we omit to avoid a heavy notation.

2. The boundary layer

The region $\mathcal{R}_1 \setminus \mathcal{R}_1(a_{12})$ is often called a boundary layer. The simplification (4.3) only occurs when $\boldsymbol{r}_1$ is not in this boundary layer, that is when $\boldsymbol{r}_1 \in \mathcal{R}_2(a_{12})$. This is because then $\partial\mathcal{R}_2 \cap \partial\mathcal{B}(\boldsymbol{r}; a_{12}) = \varnothing$, and therefore the boundary of $\mathcal{R}_2 \setminus \mathcal{B}(\boldsymbol{r}_1; a_{12})$ becomes $\partial\mathcal{R}_2 \cup \partial\mathcal{B}(\boldsymbol{r}_1; a_{12})$.

In this paper we will not discuss how to evaluate the system (3.17) for $\boldsymbol{r}_1 \in \mathcal{R}_1 \setminus \mathcal{R}_1(a_{12})$. Evaluating in this boundary layer is used to combine the different fields $f_{p,n}$, but this is only needed for very strong multiple-scattering [25, 26]. We also note that for a slab geometry, it is possible to evaluate the complex integrals when $\boldsymbol{r}_1$ is located in the boundary layer, see [33, 35].

By substituting equations (4.1)–(4.5) into the governing equation (3.17), and assuming $\boldsymbol{r}_1 \in \mathcal{R}_2(a_{12})$, we obtain

$$\sum_p f_{p,n}(\boldsymbol{r}_1, \lambda_1) = \sum_{n'} T_n(\lambda_1)\mathcal{V}_{n'n}(k\boldsymbol{r}_1)g_{n'} + \sum_{n'p} T_n(\lambda_1) \int_{\mathcal{S}} \frac{\mathcal{I}_{p,n'n}(\boldsymbol{r}_1) - \mathcal{J}_{p,n'n}(\boldsymbol{r}_1)}{k^2 - k_p^2} \bar{\mathfrak{n}}(\lambda_2) \mathrm{d}\lambda_2, \quad \boldsymbol{r}_1 \in \mathcal{R}_2(a_{12}), \tag{4.6}$$

where we number the p indices in the order $p = 1, 2, \ldots, \infty$, though we will see later that only a few are needed to obtain accurate results.

The key to simplifying (4.6) is to note that both $f_{p,n}(\boldsymbol{r}_1)$ and $\mathcal{J}_{p,n'n}(\boldsymbol{r}_1)$ satisfy a wave equation with wavenumber k_p and spatial position $\boldsymbol{r}_1$, whereas $\mathcal{V}_{n'n}(k\boldsymbol{r}_1)$ and $\mathcal{I}_{p,n'n}(\boldsymbol{r}_1)$ satisfy a wave equation with wavenumber k. This enables us to use Theorem C.1 to conclude that

$$f_{p,n}(\boldsymbol{r}_1, \lambda_1) + \sum_{n'} \frac{T_n(\lambda_1)}{k^2 - k_p^2} \int_{\mathcal{S}} \mathcal{J}_{p,n'n}(\boldsymbol{r}_1) \bar{\mathfrak{n}}(\lambda_2) \mathrm{d}\lambda_2 = 0, \qquad \text{(the ensemble wave equation)} \tag{4.7}$$

$$\sum_{n'} \mathcal{V}_{n'n}(k\boldsymbol{r}_1)g_{n'} + \sum_{n'p} \int_{\mathcal{S}} \frac{\mathcal{I}_{p,n'n}(\boldsymbol{r}_1)}{k^2 - k_p^2} \bar{\mathfrak{n}}(\lambda_2) \mathrm{d}\lambda_2 = 0, \qquad \text{(the ensemble boundary conditions)} \tag{4.8}$$

both valid for $\boldsymbol{r}_1 \in \mathcal{R}_1(a_{12})$. We emphasize that the sum over p, which was present in (4.6), has now disappeared because each of the $f_{p,n}(\boldsymbol{r}_1)$ for $p = 1, 2, \ldots$ satisfies a wave equation with a different wavenumber.

Now it is clear that (4.7) is independent of both *the region of particles* $\mathcal{R}_j$ and *the incident field*. We will show how the effective wavenumbers k_p can be completely determined from (4.7). On the other hand, equation (4.8) depends on both the region and incident wave, and will lead to a restriction on how to combine the $f_{p,n}(\boldsymbol{r}, \lambda)$. Equation (4.8) is sometimes called the extinction equation.

Both (4.7) and (4.8) can be further simplified by expanding the fields in terms of orthonormal functions, which we do in the section below.

5 The dispersion equation

The effective wavenumbers k_p and much about the fields $f_{p,n}(\boldsymbol{r}_1, \lambda_1)$, can be calculated just from the ensemble wave equation (4.7). Depending on the symmetries of $f_{p,n}(\boldsymbol{r}_1, \lambda_1)$ we can reach different dispersion equations, the most general of which just assumes that $f_{p,n}(\boldsymbol{r}_1, \lambda_1)$ is a smooth field.

5.1 Effective regular waves

Here, we determine the effective wavenumbers k_p from the ensemble wave equation (4.7). To do so, we use an origin O, for our coordinate system, located in $\mathcal{R}_2(a_{12})$, and we expand $f_{p,n}(\boldsymbol{r}_1, \lambda_1)$ in a series of regular spherical functions of the wave equation in the domain $\mathcal{R}_2(a_{12})$. We note that convergence of this regular expansion is guaranteed within a sphere, see Appendix G, which is all we will require below to reach an equation for the effective wavenumbers.

This regular series takes the form:

$$f_{p,n}(\boldsymbol{r}_1,\lambda_1)=\sum_{n_1}F_{p,nn_1}(\lambda_1)\mathrm{v}_{n_1}(k_p\boldsymbol{r}_1), \tag{5.1}$$

$$f_{p,n}(\boldsymbol{r}+\boldsymbol{r}_1,\lambda_2)=\sum_{n_1n_2}F_{p,nn_1}(\lambda_2)\mathcal{V}_{n_1n_2}(k_p\boldsymbol{r})\mathrm{v}_{n_2}(k_p\boldsymbol{r}_1), \tag{5.2}$$

where the coefficients $F_{p,nn_1}(\lambda_1)$ are to be determined, and we used the translation matrix $\mathcal{V}_{n_1n_2}(k_p\boldsymbol{r})$ in the second expansion. The convergence of this series depends on the behaviour of the expansion coefficients $F_{p,nn_1}(\lambda_1)$, which in turn depend on both the confining geometry and the incident field. At this stage, we assume the series is convergent. In Appendix D we show how substituting the above into the dispersion equation (4.7) leads to

$$\sum_{n_1}F_{p,nn_1}(\lambda_1)\mathrm{v}_{n_1}(k_p\boldsymbol{r}_1)+\sum_{n_2}G_{n,n_2}(\lambda_1)\mathrm{v}_{n_2}(k_p\boldsymbol{r}_1)=0, \tag{5.3}$$

where

$$G_{n,n_2}(\lambda_1)=\frac{T_n(\lambda_1)}{k_p^2-k^2}\sum_{n_1n_3n'}c_{nn'n_3}c_{n_1n_2n_3}\int_{\mathcal{S}}a_{12}\mathrm{N}_{\ell_3}(ka_{12},k_pa_{12})F_{p,n'n_1}(\lambda_2)\mathfrak{n}(\lambda_2)\,\mathrm{d}\lambda_2 \tag{5.4}$$

where the $c_{n'nn_1}$ are numbers which are defined in Appendix B, and

$$\mathrm{N}_\ell(x,z)=x\mathrm{h}_\ell^{(1)\prime}(x)\mathrm{j}_\ell(z)-z\mathrm{h}_\ell^{(1)}(x)\mathrm{j}_\ell'(z). \tag{5.5}$$

By using the orthonormal property of spherical harmonics (5.3) reduces to

$$F_{p,nn_2}(\lambda_1)+G_{n,n_2}(\lambda_1)=0. \qquad \text{(the regular eigen-system)} \tag{5.6}$$

The above is a linear equation, for all n, n_2, and λ_1, which can be solved for the unknown $F_{p,n'n_1}(\lambda_1)$. For example, if we discretise the functions $F_{p,n'n_1}(\lambda_1)$and $G_{n,n_2}(\lambda_1)$ in λ_1, we could then represent them with the vector $\mathbf{F}$ and the matrix $\mathbf{G}$, respectively, and rewrite the above in the form

$$(\mathbf{I}+\mathbf{G})\mathbf{F}=0\implies\det(\mathbf{I}+\mathbf{G})=0, \tag{5.7}$$

where the second equations holds for a non-zero $\mathbf{F}$. This determinant equation can be used to find all effective wavenumbers k_p, which do not depend on the material geometry. Although (5.7) contains all possible effective wavenumbers it is computationally simpler to solve the planar dispersion equation which also contains all viable effective wavenumbers, as we will show below. Solving (5.7) can be numerically difficult for two reasons: 1) there are many different wavenumbers k_p which are solutions to (5.7), and each of these k_p can have different multiplicities, and 2) there are many spurious roots, as discussed in the optional box below.

The plane wave dispersion, and other reduced dispersion equations, are calculated by restricting the form of $f_{p,n}(\boldsymbol{r}_1,\lambda_1)$ through the use of symmetry reductions as shown in Section 3.4.

3. Spurious wavenumbers k_p

One problem with using (5.7) to find the wavenumbers k_p is that (5.7) has spurious roots. That is, it has solutions k_p which are not solutions to the ensemble wave equation (4.7). Figure 4 shows some of these spurious solutions. The example examples/equivalent-symmetries in [29] gives code to calculate these spurious wavenumbers.

These spurious solutions appear when truncating the index n_2 in F_{p,nn_2} and then solving (5.7). Calculating the eigenvectors F_{p,nn_2} of these spurious solutions k_p would then lead the series in (5.1) to rapidly diverge, which is physically not viable. That is, when truncating the system (5.6) for $\ell_2\leq L_2$, it would also be natural to truncate $\ell_1\leq L_2$. However, neglecting the terms $F_{p,n'n_1}$ with $\ell_1>L_2$ on the right hand-side of (5.6) is only approximately correct if $|F_{p,n'n_1}|$ is small or at least getting smaller when increasing ℓ_1. These spurious roots k_p on the other hand lead to $|F_{p,n'n_1}|$ which increase with ℓ_1.

5.2 Effective azimuthal waves

When both the incident wave and material region share a rotational symmetry around the $z-$axis we can reach a reduced representation of $f_{p,n}(\boldsymbol{r}_1,\lambda_1)$ by using (3.19). For example, this occurs when the incident wave is $u_{\mathrm{in}}(\boldsymbol{r})=\mathrm{e}^{\mathrm{i}kz}$ and the material region is a sphere centred at the origin.

Combining the symmetry (3.19) with the representation (5.1) leads to the form

$$f_{p,n}(\boldsymbol{r}_1,\lambda_1)=\sum_{\ell_1\geq|m|}F_{p,n\ell_1}(\lambda_1)\mathrm{v}_{(\ell_1,-m)}(k_p\boldsymbol{r}_1), \tag{5.8}$$

where $F_{p,n\ell_1}=F_{p,n(\ell_1,-m)}$. In other words, in terms of the representation (5.1) we have that $F_{p,nn_1}=0$ unless $m_1=-m$ and $\ell_1\geq|m|$.

Substituting (5.8) into (5.6) then leads to

$$F_{p,n\ell_2}(\lambda_1)+G_{n,(\ell_2,-m)}(\lambda_1)=0\quad\text{for every } n,\ \ell_2\geq|m|, \tag{5.9}$$

which is a restricted version of (5.7). Note that for the above, in the sum (5.4) we should set $m_1=-m'$ and sum over $\ell_1\geq|m'|$. Further (5.6) also leads to $G_{n,n_2}(\lambda_1)=0$ for every $m_2\neq-m$, but this is automatically satisfied because $c_{nn'n_3}c_{(\ell_1,-m')(\ell_2,m_2)n_3}=0$ when $m_2\neq-m$.

5.3 Effective plane-waves

Here, we restrict $f_{p,n}(\boldsymbol{r}_1,\lambda_1)$ by imposing planar symmetry (3.21). This will allow us to deduce simpler dispersion equations, as well as deduce reflection and transmission from a plate.

By combining the symmetry (3.21) with the wave equation (4.1) we first conclude that

$$f_{p,n}(\boldsymbol{r}_1,\lambda_1)=F_{p,n}(\lambda_1)\mathrm{e}^{\mathrm{i}\boldsymbol{k}_p\cdot\boldsymbol{r}_1}, \tag{5.10}$$

where $\boldsymbol{k}_p\cdot\boldsymbol{r}_1$ is simply a sum of element wise multiplication without conjugation, even though $\boldsymbol{k}_p$ is a complex vector.

In the appendix E we show that substituting the above into (4.7) leads to

$$F_{p,n}(\lambda_1)+\sum_{n'n_1}\frac{4\pi c_{n'nn_1}}{k_p^2-k^2}\mathrm{i}^{-\ell_1}\mathrm{Y}_{n_1}(\hat{\boldsymbol{k}}_p)T_n(\lambda_1)\int_{\mathcal{S}}a_{12}\mathrm{N}_{\ell_1}(ka_{12},k_pa_{12})F_{p,n'}(\lambda_2)\bar{\mathfrak{n}}(\lambda_2)\mathrm{d}\lambda_2=0, \tag{5.11}$$

and that, when considering only one type of particle, the above reduces to an equation which is found in much of the literature [38, 18, 56, 41, 15, 28].

Note that

$$\hat{\boldsymbol{k}}_p=(\sin\theta_p\cos\phi_p,\sin\theta_p\sin\phi_p,\cos\theta_p)\quad\text{and}\quad Y_{n_1}(\hat{\boldsymbol{k}}_p)=Y_{n_1}(\theta_p,\phi_p), \tag{5.12}$$

and the angles θ_p and ϕ_p can be complex numbers, meaning that we may have $|\hat{\boldsymbol{k}}_p|\neq1$, but we do have that $\hat{\boldsymbol{k}}_p\cdot\hat{\boldsymbol{k}}_p=1$ for the real inner product.

Equation (5.11) can be turned into a determinant equation, much like (5.7), from which we can calculate effective wavenumbers k_p:

$$(\mathbf{I}+\mathbf{C})\mathbf{F}=0\implies\det(\mathbf{I}+\mathbf{C})=0. \tag{5.13}$$

The form of the eigensystem (5.11) seems to suggest that the k_p depend on $\hat{\boldsymbol{k}}_p$. However, a direct (though cumbersome) evaluation of the resulting (truncated) determinant system would confirm that $\hat{\boldsymbol{k}}_p$ has no contribution. Further, the more general eigensystem (5.6) does not depend on $\hat{\boldsymbol{k}}_p$. As a sanity check, we can explicitly show that every solution to (5.11) is also a solution to (5.6). To achieve this we rewrite the solution (5.10) in the form (5.1) by using a plane-wave expansion (A.2) in (5.10) to obtain:

$$f_{p,n}(\boldsymbol{r}_1,\lambda_1)=\sum_{n_1}F_{p,nn_1}(\lambda_1)\mathrm{v}_{n_1}(k_p\boldsymbol{r}_1)\quad\text{with}\quad F_{p,nn_1}(\lambda_1)=4\pi\mathrm{i}^{\ell_1}(-1)^{m_1}F_{p,n}(\lambda_1)\mathrm{Y}_{(\ell_1,-m_1)}(\hat{\boldsymbol{k}}_p). \tag{5.14}$$

Because the above is in the form (5.1) and the field $f_{p,n}(\boldsymbol{r}_1,\lambda_1)$ satisfies the general dispersion equation (4.7) (when (5.11) is satisfied) then F_{p,nn_1} and k_p must also satisfy the regular eigensystem (5.6).

As the k_p are independent of $\hat{\boldsymbol{k}}_p$, we can choose any $\hat{\boldsymbol{k}}_p$ to calculate the k_p. We exemplify for just one type of particle[5]: take $\hat{\boldsymbol{k}}_p=\hat{\boldsymbol{z}}$ so that $Y_{n_1}(\hat{\boldsymbol{k}}_p)=\sqrt{2\ell_1+1}/\sqrt{4\pi}\delta_{m_10}$, then the k_p must satisfy

$$\det(M_{nn'}(k_p))=0,\quad\text{where} \tag{5.15}$$

$$M_{nn'}(k_p)=\delta_{nn'}+\sum_{\ell_1}\frac{\sqrt{4\pi}c_{n'n(\ell_1,0)}}{k_p^2-k^2}\mathrm{i}^{-\ell_1}\sqrt{2\ell_1+1}T_n\bar{\mathfrak{n}}a_{12}\mathrm{N}_{\ell_1}(ka_{12},k_pa_{12})=0,$$

[5] We chose not to show the version valid for many difference particles properties λ_2 because it would require discretising the integral over λ_2.

where $\bar{\mathfrak{n}} = \mathfrak{n}(N-1)/N$ and $\mathfrak{n}$ is the number density of particles. This equation can be even further simplified when there is azimuthal symmetry, as is the case for the incident plane-wave $\mathrm{e}^{\mathrm{i}kz}$ and material region $z > 0$. In this case we can apply the symmetry (3.22) to (5.15) and reach

$$\det(M_{(\ell,0)(\ell',0)}(k_p)) = 0. \tag{5.16}$$

All the k_p that satisfy (5.16) also satisfy (5.15), however, there are solutions to (5.15) which do *not* satisfy (5.16), see Figure 4. That is, it is not possible to excite all effective wavenumbers when considering only direct incidence $u_{\mathrm{in}}(\boldsymbol{r}) = \mathrm{e}^{\mathrm{i}kz}$. In other words, one type of experiment (one type of incident wave and material geometry) can only excite a portion of all the effective wavenumbers[6].

5.4 Plane-wave dispersion has all viable effective wavenumbers

Because the representation (5.1) is more general than a plane-wave representation (5.10), we know that all solutions k_p to the plane-wave dispersion (5.13) must also satisfy the more general regular dispersion (5.6). There is even an explicit conversion from plane-wave solutions to the regular solutions (5.14). However, it is not at all obvious that all viable solutions k_p of the regular dispersion (5.6) must satisfy plane-wave dispersion (5.13).

To show that all viable wavenumbers k_p that satisfy the regular dispersion (5.7) must also satisfy the plane-wave dispersion (5.13), we need to rewrite the expansion (5.1) in terms of plane-waves. We achieve this by using [36]

$$\mathrm{v}_{n_1}(k_p\boldsymbol{r}_1) = \frac{1}{4\pi\mathrm{i}^{\ell_1}}\int_{\Omega_q} \mathrm{Y}_{n_1}(\hat{\boldsymbol{q}})\mathrm{e}^{\mathrm{i}k_p\hat{\boldsymbol{q}}\cdot\boldsymbol{r}}\,\mathrm{d}\Omega_q, \tag{5.17}$$

where Ω_q is the solid angle of the radial unit vector $\hat{\boldsymbol{q}}$. The above can be verified by using a plane-wave expansion (A.2) for $\mathrm{e}^{\mathrm{i}k_p\hat{\boldsymbol{q}}\cdot\boldsymbol{r}_1}$, to write

$$f_{p,n}(\boldsymbol{r}_1,\lambda_1) = \int_{\Omega_q} F_{p,n}(\hat{\boldsymbol{q}},\lambda_1)\mathrm{e}^{\mathrm{i}k_p\hat{\boldsymbol{q}}\cdot\boldsymbol{r}_1}\,\mathrm{d}\Omega_q, \tag{5.18}$$

where

$$F_{p,n}(\hat{\boldsymbol{q}},\lambda_1) = \frac{1}{4\pi}\sum_{n_1} F_{p,nn_1}(\lambda_1)\mathrm{i}^{-\ell_1}\mathrm{Y}_{n_1}(\hat{\boldsymbol{q}}). \tag{5.19}$$

Written in this form, $f_{p,n}(\boldsymbol{r}_1,\lambda_1)$ is now a superposition of plane waves all with the same wavenumber k_p but with different directions $\hat{\boldsymbol{q}}$. Note that the F_{p,nn_1} depend on k_p but are independent of the $\hat{\boldsymbol{q}}$. To find a dispersion equation we can repeat the same steps that led to (5.11) to reach:

$$\int_{\Omega_q}\left[F_{p,n}(\hat{\boldsymbol{q}},\lambda_1) + \sum_{n'n_1}\frac{4\pi c_{n'nn_1}}{k_p^2-k^2}\mathrm{i}^{-\ell_1}\mathrm{Y}_{n_1}(\hat{\boldsymbol{q}})T_n(\lambda_1)\int_{\mathcal{S}} a_{12}\mathrm{N}_{\ell_1}(ka_{12},k_pa_{12})F_{p,n'}(\hat{\boldsymbol{q}},\lambda_2)\bar{\mathfrak{n}}(\lambda_2)\,\mathrm{d}\lambda_2\right] \times \mathrm{e}^{\mathrm{i}k_p\hat{\boldsymbol{q}}\cdot\boldsymbol{r}_1}\,\mathrm{d}\Omega_q = 0. \tag{5.20}$$

As the map $\hat{\boldsymbol{q}} \to F_{p,n}(\hat{\boldsymbol{q}},\lambda_1)$ is smooth, we can conclude that the integrand in the above is also a smooth function of $\hat{\boldsymbol{q}}$, in which case, the above can only be zero for every $\boldsymbol{r}_1$ when the integrand is zero for every $\hat{\boldsymbol{q}}$. That is, the k_p and $F_{p,n}(\hat{\boldsymbol{q}},\lambda_1)$ have to satisfy the plane-wave dispersion equation (5.11), with the same k_p for every $\hat{\boldsymbol{q}}$, which in turn implies that k_p has to satisfy the determinant equation (5.13).[7]

5.5 Effective properties in the long wavelength limit

By taking the limit where the incident wavelength is long compared to the particle diameter, we can calculate the effective properties directly from any of the dispersion equations. This procedure is explained in detail in [52, 46, 28].

It is particularly interesting to calculate the effective properties from the regular dispersion equation (5.7), because this equation holds for any material geometry, which then gives us confidence that the effective properties are truly properties of the material's microstructure and medium, and not its geometry.

[6] Note this does *not* mean there exist wavenumbers k_p that change (continuously) with the angle of incidence $\hat{\boldsymbol{k}}_p$. There are, however, solutions k_p which are not excited for certain angles of incidence.

[7] In more detail, let $\int_{\Omega_k} f(\hat{\boldsymbol{k}})\mathrm{e}^{\mathrm{i}k\hat{\boldsymbol{k}}\cdot\boldsymbol{r}}\,\mathrm{d}\Omega_k = 0, \forall \boldsymbol{r} \in \mathcal{R}$, and expand $f(\hat{\boldsymbol{k}})$ in spherical harmonics, *i.e.*, $f(\hat{\boldsymbol{k}}) = \sum_n f_n \mathrm{Y}_n(\hat{\boldsymbol{k}})$. We assume this relation holds in a ball of radius R, centred at the origin. Then, using the transformation (5.17), we obtain $\sum_n \mathrm{i}^\ell f_n \mathrm{v}_n(k\boldsymbol{r}) = 0, \forall \boldsymbol{r} \in \mathcal{R}$. Orthogonality of the spherical harmonics implies $f_n \mathrm{j}_\ell(kr) = 0, r \in [0,R], \forall n$, and $f_n = 0$, since the zeros of the spherical Bessel functions are isolated points on the real axis.

Here we calculate the effective properties for spherical particles (2.8) and acoustics. To achieve this, we need to consider the limit $k \to 0$, starting with the T-matrix coefficients which scale with k in the form

$$T_{(0,0)}(\lambda_j) \sim \frac{\mathrm{i}k^3 a_j^3}{3}\Delta\beta_j, \quad T_{(1,m)}(\lambda_j) \sim -\frac{\mathrm{i}k^3 a_j^3}{3}\Delta\rho_j \quad \text{for } m = -1, 0, 1, \tag{5.21}$$

and $T_{(\ell,m)}(\lambda_j) \sim 0$ for $\ell > 1$, where

$$\Delta\rho_j = \frac{\rho - \rho_j}{\rho + 2\rho_j} \quad \text{and} \quad \Delta\beta_j = \frac{\beta - \beta_j}{\beta_j},$$

with $\beta_j = \rho_j\omega^2/k_j^2$ and $\beta = \rho\omega^2/k^2$ being the bulk modulus of the j-th particle and of the background medium, respectively. For particles with any shape, there is a similar result for their T-matrix when assuming that they scatter only monopole and dipole waves[60].

To facilitate the next steps, we rewrite the effective wavenumber k_* and expand

$$k_* = \frac{k}{c_*}\sqrt{\frac{\beta}{\rho}} \quad \text{and} \quad \mathrm{N}_\ell(ka_{12}, k_*a_{12}) \sim \frac{\mathrm{i}}{ka_{12}c_*^\ell}\left(\frac{\beta}{\rho}\right)^{\ell/2},$$

where c_* is the constant effective phase speed.

The expansion (5.21) for the T_n imply that, at leading order in small k, only F_{p,nn_1} for $n = (0,0), (1,-1), (1,0), (1,1)$ has a significant contribution, with all other terms being zero. We will also truncate ℓ_1 in F_{p,nn_1} by assuming $\ell_1 \leq L$ for some $L \geq 2$.

By substituting the above into (5.7), and then expanding up to leading order in small k, we find *three* possible solutions for the effective phase speed c_*. Two of these solutions are non-physical, because they do not satisfy the plane-wave dispersion, as discussed in Section 5.4 and in the optional box (3). There is therefore only one viable low frequency wavespeed c_* remaining which means that, as expected, the particles act as one homogeneous material in the long wavelength limit. This effective wavespeed is given by

$$c_*^2 = \frac{\beta}{1 + \langle\Delta\beta_j\rangle}\frac{1}{\rho}\frac{1 + 2\langle\Delta\rho_j\rangle}{1 - \langle\Delta\rho_j\rangle}, \qquad \text{(effective phase speed)} \tag{5.22}$$

where, just for this section, we define

$$\langle\Delta\beta_j\rangle = \int_{\mathcal{S}} \Delta\beta_j\bar{\varphi}(\lambda_j)d\lambda_j,$$

and likewise for $\Delta\rho_j$, where $\bar{\varphi}(\lambda_j)\,\mathrm{d}\lambda_j$ is the volume fraction of particles with the properties λ_j, so that $\int_{\mathcal{S}} \bar{\varphi}(\lambda_j)\,\mathrm{d}\lambda_j = \bar{\varphi}$, the total particle volume fraction. Note that for spheres $\bar{\varphi}(\lambda_j) = \frac{4\pi a_j^3}{3}\bar{\mathfrak{n}}(\lambda_j)$.

By writing $c_*^2 = \beta_*/\rho_*$ we can now identify the effective bulk modulus β_* and density ρ_* as

$$\frac{1}{\beta_*} = \frac{1}{\beta} + \frac{\langle\Delta\beta_j\rangle}{\beta} \quad \text{and} \quad \rho_* = \rho\frac{1 - \langle\Delta\rho_j\rangle}{1 + 2\langle\Delta\rho_j\rangle}. \qquad \text{(effective properties)} \tag{5.23}$$

When considering only one type of particle, that above reduces to a classical formula given by [3, equation (9)] (in the absence of viscosity) and many others [46]. When performing this same procedure for the plane-wave dispersion equation (5.11) or for azimuthal symmetry (5.9) we recover the same effective properties. Also note, that for only one type of particle, with the properties β_1 and ρ_1, we recover the correct limits: when $\varphi \to 0$ we get $\beta_* \to \beta$ and $\rho_* \to \rho$, and when $\varphi \to 1$ we get $\beta_* \to \beta_1$ and $\rho_* \to \rho_1$.

5.6 Numerical effective wavenumbers

Here we numerically explore the effective wavenumbers which solve the dispersion equations: (5.7) with azimuthal symmetry (5.8), planar symmetry (5.15), and the combined planar with azimuthal symmetry (5.16). Code to reproduce our results is available in the package [29].

The material properties we use in this section are shown in Table 1.

$\varphi = 30\%$	(particle volume fraction)
$ka_o = \pi/8$	(non-dimensional particle radius)
$\rho_o/\rho = c_o/c = 0.1$	(void particle properties)
$\rho_o/\rho = c_o/c = 10.0$	(solid particle properties)

Table 1: For numerical experiments we use identical spherical particles with the T-matrix (2.8) and the material properties given above, where $c = \omega/k$ and $c_o = \omega/k_o$ are the background and particle wave speed, respectively. Note that we give the properties of the particles relative to the background properties. The properties of the void particle are an example of strong scatterers, while that of the solid particle are an example of weak scatterers.

4. Algorithm - effective wavenumbers

A minimal algorithm to calculate the effective wavenumbers k_p for any material region. Code to calculate these wavenumbers is given in manual/wavenumbers as part of the package [29].

1. Choose the particle statistics by choosing:
   - 1.1. a wavenumber k, where $\omega = ck$ and c is the background wave speed.
   - 1.2. the coefficients of the T-matrix T_n. One example is given by (2.8).
   - 1.3. the function $p(\lambda_1)$ detailed in Section 3.1. For just one type of particle, or specie, $p(\lambda_1) = \delta(\lambda_1 - \lambda^*)$.
   - 1.4. the exclusion distance a_{12}, with $a_{12} = 1.001(a_1 + a_2)$ being a common choice.
2. Choose a truncation $\ell \leq L$, for the ℓ in $n = (\ell, m)$ and in F_{p,nn_1} or $F_{p,n}$ based on how the T_n decay.
3. Calculate the effective wavenumbers k_p by solving (5.16) or (5.15).

In Figures 4-5 we show the result of using Algorithm 4 above to calculate the different effective wavenumbers when using the properties in Table 1. In both cases, the wavelength λ is sixteen times larger than the particle radius. The important messages to take-away from these figure are:

1. The more general regular dispersion equation has spurious roots, which are the ones that do not satisfy the planar dispersion, as discussed in Section 5.4. An example of four of these spurious roots are shown in Figure 4 with the label Azi.
2. There can be two effective wavenumbers with lower imaginary part (and are not spurious roots), as shown in Figure 4. These two will dominate the ensemble average transmission and scattering, as the other wavenumbers will be very difficult to excite. For weaker scatterers there tends to be only one wavenumber with lower imaginary part as shown in Figure 5.
3. The simpler combined planar-azimuthal dispersion (5.16) equation contains the two most important wavenumbers. This seems to hold in general.
4. Many of the effective wavenumbers have a negative real part, meaning that they travel backwards in the opposite direction to the incident wave. This is an usual prediction from the theory, but is completely physically viable.

We remark that in many cases, including the limits of low frequency, low volume fraction, and weak scatterers, we find there is only one wavenumber with a low imaginary part, and knowing this wavenumber is often enough to accurately calculate the ensemble average transmission and scattering [26, 25]. These findings are based on some analytic results, but mostly numerical investigations. A complete understanding on exactly how accurate these solutions are is still unresolved.

6 Scattering from a sphere filled with particles

If one effective wavenumber k_1 has a significantly smaller imaginary part than the other wavenumbers, e.g. Im $k_1 \ll$ Im k_p for $p = 2, 3, \ldots$, then $\langle f_n \rangle(\boldsymbol{r}_1, \lambda_1) \approx f_{1,n}(\boldsymbol{r}_1, \lambda_1)$, where $f_{1,n}(\boldsymbol{r}_1, \lambda_1)$ is the wavemode associated with k_1 as shown in the representation (4.1). This occurs for a number of scenarios including: weak scattering, low frequency, or low volume fraction [26, 25].Beyond these cases $\langle f_n \rangle(\boldsymbol{r}_1, \lambda_1) \approx f_{1,n}(\boldsymbol{r}_1, \lambda_1)$ has been numerically [26] observed. For now we take this as an unproven hypothesis.

When using only one effective wavenumber, we can explicitly calculate the average scattered and transmitted waves for many different material geometries. To achieve this, for each material geometry, we specialise the average

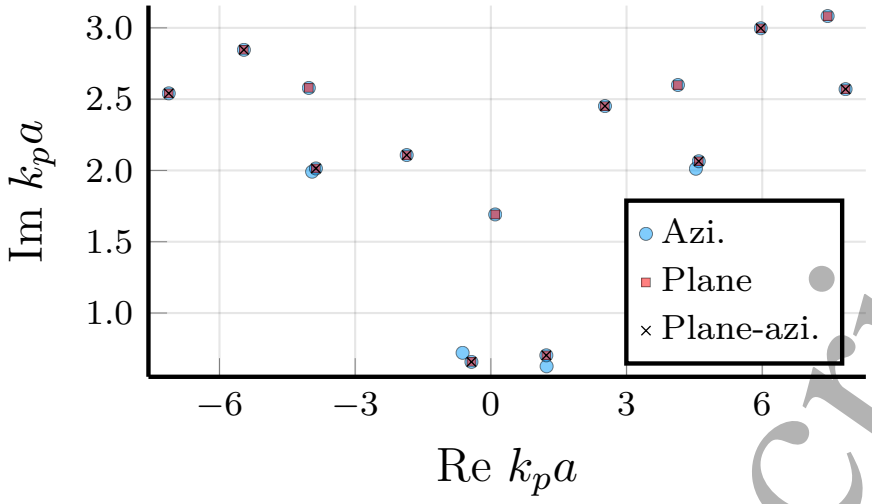

Figure 4: The effective wavenumbers that satisfy azimuthal symmetry (5.9), the planar dispersion (5.15), or the combined planar with azimuthal dispersion (5.16). Note there are four wavenumbers k_p that satisfy (5.9) but do not satisfy (5.15) or (5.16). These are non-physical spurious roots as discussed in the optional box (3). We used the material properties in Table 1 for void particles and incident wavenumber times particle radius $ka_o = \pi/8$, which means the wavelength is 16 times longer than the particle radius. See examples/equivalent-symmetries in [29] for code to produce these results.

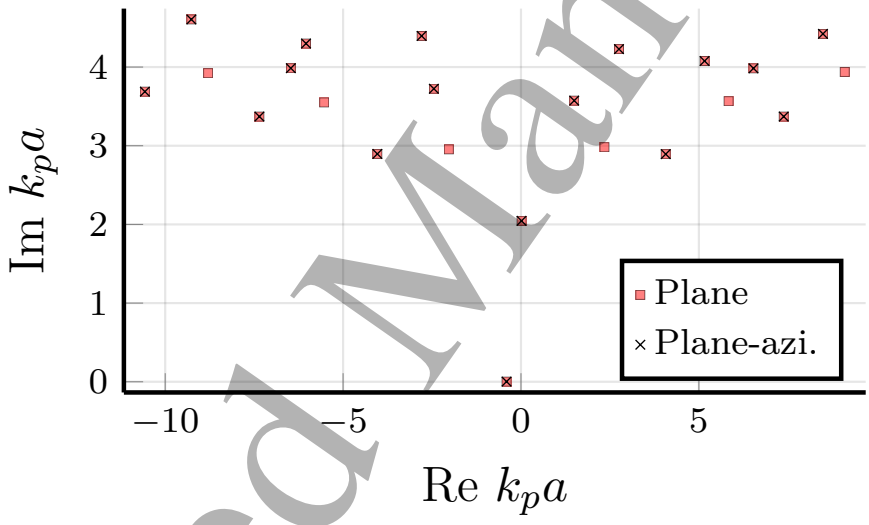

Figure 5: The effective wavenumbers that satisfy the planar dispersion (5.15) or the combined planar with azimuthal dispersion (5.16). Note that the wavenumber closest to the real axis will be the most important, as it has a smaller imaginary part. We used the material properties in Table 1 for solid particles and incident wavenumber times particle radius $ka_o = \pi/8$. See manual/wavenumbers in [29] for code to produce these results.

scattered wave (3.15) to the material geometry, then use the average boundary conditions (4.8) to restrict the wavemode $f_{1,n}(\boldsymbol{r}_1, \lambda_1)$. With the wavemode we can calculate both the average scattered and transmitted wave, although transmission requires some extra steps [44].

In this section, we calculate the average scattered wave from a sphere filled with particles. To our knowledge, the sphere case has never been analytically calculated in all its details, though there have been approximate methods [51] and numerical methods that simulate a large number of configurations [43, 42, 41].

6.1 The average boundary conditions

We assume that all particles are confined in a sphere of radius R which implies that the particle origins $\mathcal{R}_1 = \{\boldsymbol{r}_1 \in \mathbb{R}^3 : |\boldsymbol{r}_1| \leq R - a_1\}$, and let the centre of the sphere be the origin of the coordinate system for $\boldsymbol{r}_1$. Choosing a simple geometry allows us to explicitly calculate the average boundary conditions (4.4). Assume that the k_p have been determined from (5.15) and that the F_{p,nn_1}, up to a multiplying constant α_p, have been determined from (5.7). The results below can be used to completely determine, or just restrict, the α_p.

Let $\bar{R}_2 = R - a_2$, then

$$\begin{aligned}\mathcal{I}_{p,n'n}(\boldsymbol{r}_1) &= \sum_{n_1} \alpha_p F_{p,n'n_1}(\lambda_2) \int_{r=\bar{R}_2} \mathcal{U}_{n'n}(k\boldsymbol{r}_1 - k\boldsymbol{r}_2) \frac{\partial \mathrm{v}_{n_1}(k_p\boldsymbol{r}_2)}{\partial \boldsymbol{\nu}_2} - \frac{\partial \mathcal{U}_{n'n}(k\boldsymbol{r}_1 - k\boldsymbol{r}_2)}{\partial \boldsymbol{\nu}_2} \mathrm{v}_{n_1}(k_p\boldsymbol{r}_2) \mathrm{d}A_2 \\ &= -\bar{R}_2 \sum_{n_1 n_2} \alpha_p F_{p,n'n_1}(\lambda_2) c_{n'nn_2} \mathcal{V}_{n_2,(l_1,-m_1)}(k\boldsymbol{r}_1) \mathrm{N}_{l_1}(k\bar{R}_2, k_p\bar{R}_2)(-1)^{l_1+m_1} \\ &= \sum_{n_1 n_2} \bar{R}_2 \mathrm{N}_{l_1}(k\bar{R}_2, k_p\bar{R}_2) \alpha_p F_{p,n'n_1}(\lambda_2) B_{nn_2,n'n_1} \mathrm{v}_{n_2}(k\boldsymbol{r}_1) \quad \text{for } |\boldsymbol{r}_1| \leq \bar{R}_2 - a_{12}, \end{aligned} \tag{6.1}$$

where we used the translation matrices (B.3) to write $\mathcal{U}_{n'n}(k\boldsymbol{r}_1 - k\boldsymbol{r}_2) = \sum_{n_1} c_{n'nn_1} \mathrm{u}_{n_1}(k\boldsymbol{r}_1 - k\boldsymbol{r}_2) = \sum_{n_1 n_2} c_{n'nn_1} \mathcal{V}_{n_1 n_2}(k\boldsymbol{r}_1) \mathrm{u}_{n_2}(-k\boldsymbol{r}_2)$, which relied on $|\boldsymbol{r}_1| < \bar{R}_2 - a_{12} < |\boldsymbol{r}_2| = \bar{R}_2$, we then used the orthogonality of the spherical harmonics to resolve the integral, defined

$$B_{nn_2,n'n_1} = -\sum_{n_3} c_{n'nn_3} c_{n_2 n_1 n_3}, \tag{6.2}$$

and used $c_{n_3(\ell_1,-m_1)n_2} = c_{n_2 n_1 n_3}(-1)^{\ell_1+m_1}$. Substituting the above into (4.8) leads to

$$\mathbf{B} \sum_p \alpha_p \boldsymbol{F}_p = \mathbf{L}\boldsymbol{g}, \qquad \text{(boundary conditions for a sphere)} \tag{6.3}$$

where the components of $\boldsymbol{g}$ are g_n from the expansion of the incident wave (2.3), the $\boldsymbol{F}_p$ are vectors with components

$$(\boldsymbol{F}_p)_{n'n_1} = \int_{\mathcal{S}} \frac{R - a_2}{k^2 - k_p^2} \mathrm{N}_{l_1}(kR - ka_2, k_pR - k_pa_2) F_{p,n'n_1}(\lambda_2) \bar{\mathfrak{n}}(\lambda_2) \mathrm{d}\lambda_2, \tag{6.4}$$

and again we used the translation matrices (B.3) and the orthogonality of the spherical harmonics. The vector $\boldsymbol{a}$ has the components $(\boldsymbol{a})_{n'} = a_{n'}$, and $\mathbf{L}$ and $\mathbf{B}$ are matrices with components

$$(\mathbf{L})_{nn_2,n'} = -c_{n'nn_2} \quad \text{and} \quad (\mathbf{B})_{nn_2,n'n_1} = -\sum_{n_3} c_{n'nn_3} c_{n_2 n_1 n_3}. \tag{6.5}$$

5. Sparse boundary conditions

We find that numerically (6.3) has a unique solution for the α_p when using only one effective wavenumber k_1. This occurs even though (6.3) often has far more equations than unknowns α_p. That is, the number of equations is larger than the number of effective eigenvectors P. Nonetheless, both the left and right-hand side are sparse, and mostly filled with zeros. This indicates that it is possible to transform (6.3) into a smaller equivalent system to determine the α_p.

We also note that in a plate geometry, the equivalent version of (6.3) does always lead to a unique solution for the α_p when using only one effective wavenumber [25, 26], so on physical grounds we also expect (6.3) to provide a unique solution for other geometries.

6.2 Average scattered field

Assume the particles are confined in a spherical region of radius R. For the particles to fit in this region the particle origins need to be contained within $\mathcal{R}_1 = \{\boldsymbol{r}_1 \in \mathbb{R}^3 : |\boldsymbol{r}_1| \leq R - a_1\}$, where we let the centre of the sphere be the

origin of the coordinate system for $\boldsymbol{r}_1$. In this case, by taking $|\boldsymbol{r}| > R$ we can use the wave representation (4.1), Green's second identity, and then (5.1), to reduce the average scattered wave (3.15):

$$\begin{aligned}
&\sum_{np} \int_{\mathcal{R}_1} f_{p,n}(\boldsymbol{r}_1, \lambda_1) \mathrm{u}_n(k\boldsymbol{r} - k\boldsymbol{r}_1) \mathrm{d}\boldsymbol{r}_1 \\
&= \sum_{np} \frac{1}{k^2 - k_p^2} \int_{\partial \mathcal{R}_1} \left[\frac{\partial f_{p,n}(\boldsymbol{r}_1, \lambda_1)}{\partial r_1} \mathrm{u}_n(k\boldsymbol{r} - k\boldsymbol{r}_1) - f_{p,n}(\boldsymbol{r}_1, \lambda_1) \frac{\partial \mathrm{u}_n(k\boldsymbol{r} - k\boldsymbol{r}_1)}{\partial r_1} \right] (R - a_1)^2 \mathrm{d}\Omega_1 \\
&= \sum_{n'} \mathrm{u}_{n'}(k\boldsymbol{r}) \mathfrak{F}_{n'}(\lambda_1)
\end{aligned}$$

where we used (B.1-B.3) to write $\mathrm{u}_n(k\boldsymbol{r} - k\boldsymbol{r}_1) = \sum_{n'n_2} c_{n'nn_2} \mathrm{v}^*_{n_2}(k^*\boldsymbol{r}_1) \mathrm{u}_{n'}(k\boldsymbol{r})$ followed by the orthogonality of the spherical harmonics, and we defined

$$\mathfrak{F}_{n'}(\lambda_1) = \sum_{npn_1} \frac{R - a_1}{k_p^2 - k^2} c_{n'nn_1} F_{p,nn_1}(\lambda_1) \mathrm{M}_{\ell_1}(k(R - a_1), k_p(R - a_1)), \tag{6.6}$$

and $\mathrm{M}_\ell(x, y) = x\mathrm{j}'_\ell(x)\mathrm{j}_\ell(y) - y\mathrm{j}_\ell(x)\mathrm{j}'_\ell(y)$. The $\mathfrak{F}_{n'}(\lambda_1)$ are the scattering coefficients of the whole spherical region (3.16). In conclusion, substituting the above into (3.15) leads to

$$\langle u_{\mathrm{sc}}(\boldsymbol{r}) \rangle = \sum_{n'} \mathrm{u}_{n'}(k\boldsymbol{r}) \int_{\mathcal{S}} \mathfrak{F}_{n'}(\lambda_1) \mathfrak{n}(\lambda_1) d\lambda_1, \quad r > R, \qquad \text{(average scattered field)} \tag{6.7}$$

where we averaged over particle rotations.

To help piece together the equations, we provide Algorithm 6 below to calculate the average scattered wave above when only one effective wavenumber k_1 has a smaller imaginary part than the others as shown in Figure 5.

6. Algorithm - average scattering from a sphere filled with particles.

This algorithm assumes one effective wavenumber has a imaginary part significantly smaller than the others. This algorithm is implemented and tested in [29], with an example given in manual/sphere.

1. Use Algorithm 4 to calculate the wavenumber k_1 with smallest imaginary part.
2. Choose a truncation $\ell_1 \leq L_1$ for the n_1 in F_{p,nn_1} based on how the M_{ℓ_1} in (3.16) decay. The range of all other indices can now be determined from these truncations and the properties (B.6).
3. Calculate the multiple eigenvectors $F_{p,nn_1}(\lambda_1)$ of k_1 by solving (5.7). From (4.1) and (5.1) we now have that $\langle f_n \rangle(\boldsymbol{r}_1, \lambda_1) = \sum_{n_1} \mathrm{v}_{n_1}(k_1\boldsymbol{r}_1) \sum_{p=1}^{P} \alpha_p F_{p,nn_1}(\lambda_1)$, where the α_p need to be determined.
4. Solve (6.3) by:
   - 4.1. setting[a] $L' = \sqrt{P} - 1$ where $\ell' \leq L'$ in $g_{n'}$. This causes the number of unknowns α_p to be equal to the number of coefficients g_n, which leads to a unique solution α_p.
   - 4.2. setting $\mathbf{A} = \mathbf{BF}$, where $\mathbf{F}\boldsymbol{\alpha} = \sum_{p=1}^{P} \mathbf{F}_p \alpha_p$, then $\boldsymbol{\alpha} = \mathbf{A}^+ \mathbf{L}\boldsymbol{g}$ where $(\boldsymbol{\alpha})_p = \alpha_p$ and $\mathbf{A}^+ = ((\mathbf{A}^T)^* \mathbf{A})^{-1} (\mathbf{A}^T)^*$ is the pseudo-inverse.
5. Finally, calculate the scattering coefficients of the whole spherical region (6.6).

Restriction to azimuthal symmetry. Substitute: $F_{p,n'n_1} = \delta_{m_1,-m'} \delta_{\ell_1 \geq |m'|} F_{p,n'\ell_1}$, to satisfy (3.19), and $a_{n'} = \delta_{m',0} a_{\ell'}$, to make the incident wave satisfy azimuthal symmetry. For an incident plane wave impinging in the $\hat{\boldsymbol{k}}$ direction $a_{n'} = 4\pi \mathrm{i}^{\ell'} Y^*_{n'}(\hat{\boldsymbol{k}})$. When solving (6.3) take $m_2 = -m$ and only evaluate $\ell_2 \geq |m|$.

[a] For azimuthal symmetry this becomes $L' = P - 1$

7 A plate filled with particles

In this section, we calculate the average reflected wave from a plate region $\mathcal{R} = \{\boldsymbol{r} \in \mathbb{R}^3 : Z_1 \leq z \leq Z_2\}$ filled with particles, and the average transmitted wave that passes through to the other side of the plate. In this case, the particle

origins are confined to the region $\mathcal{R}_1 = \{\boldsymbol{r}_1 \in \mathbb{R}^3 : Z_1 + a_1 \le z_1 \le Z_2 - a_1\}$, where Z_2 needs to be large enough so that $Z_1 + a_1 + a_{12} < Z_2 - a_1 - a_{12}$ for every particle radius a_1 and minimum inter-particle distance a_{12}. We now assume that the incident wave is a plane wave with wave-vector $\boldsymbol{k} = (k_x, k_y, k_z)$, where $k_z > 0$ (the incident wave impinges the plate from below). Further, by planar symmetry (3.21) we can also assume that $k_{p_x} = k_x$ and $k_{p_y} = k_y$.

7.1 Average transmission

We start with the transmitted field using the wave representation (3.14), (3.15), (4.1), and (5.10). By assuming that $z > Z_2$, which is the side of the plate where the transmitted wave will appear, we can use Green's second identity, as we did in Section 4.1, to reduce the average (total) transmitted wave:

$$\langle u(\boldsymbol{r})\rangle = \mathrm{e}^{\mathrm{i}\boldsymbol{k}\cdot\boldsymbol{r}} + \langle u_{\mathrm{sc}}(\boldsymbol{r})\rangle = \mathrm{e}^{\mathrm{i}\boldsymbol{k}\cdot\boldsymbol{r}} + \sum_{n,p}\int_{\mathcal{S}} \mathfrak{n}(\lambda_1)F_{p,n}(\lambda_1)\int_{\mathcal{R}_1} \mathrm{e}^{\mathrm{i}\boldsymbol{k}_p\cdot\boldsymbol{r}_1}\mathrm{u}_n(k\boldsymbol{r}-k\boldsymbol{r}_1)\,\mathrm{d}\boldsymbol{r}_1\,\mathrm{d}\lambda_1. \tag{7.1}$$

By using Green's second identity we can reduce the integral in $\boldsymbol{r}_1$ to surface integrals:

$$\int_{\mathcal{R}_1} \mathrm{e}^{\mathrm{i}\boldsymbol{k}_p\cdot\boldsymbol{r}_1}\mathrm{u}_n(k\boldsymbol{r}-k\boldsymbol{r}_1)\mathrm{d}\boldsymbol{r}_1 = \frac{\mathrm{e}^{\mathrm{i}\boldsymbol{k}_p\cdot\boldsymbol{x}}}{k^2-k_p^2}(-1)^\ell\left[L_n(Z_2-a_1-z) - L_n(Z_1+a_1-z)\right], \tag{7.2}$$

where we used a change of integration variable from $\boldsymbol{r}_1 \mapsto (\boldsymbol{r}_1 - \boldsymbol{r})$, $\mathrm{u}_n(-k\boldsymbol{r}_1) = \mathrm{u}_n(k\boldsymbol{r}_1)(-1)^\ell$, and the definition of L_n which is given by (F.1). As both $Z_2 - a_1 - z$ and $Z_1 + a_1 - z$ are negative real numbers, we can use the result (F.6) to evaluate the above and reach

$$\langle u(\boldsymbol{r})\rangle = T_{\text{plate}}\mathrm{e}^{\mathrm{i}\boldsymbol{k}\cdot\boldsymbol{r}}, \qquad \text{(average transmitted field)} \tag{7.3}$$

where

$$T_{\text{plate}} = 1 + \sum_{n,p}\int_{\mathcal{S}} \mathfrak{n}(\lambda_1)F_{p,n}(\lambda_1)\frac{(-1)^\ell}{k_z-k_{p_z}}\frac{2\pi\mathrm{i}^{\ell+1}}{kk_z}\mathrm{Y}_n(\hat{\boldsymbol{k}})\left[\mathrm{e}^{\mathrm{i}(k_{p_z}-k_z)(Z_2-a_1)} - \mathrm{e}^{\mathrm{i}(k_{p_z}-k_z)(Z_1+a_1)}\right]\mathrm{d}\lambda_1,$$

and $\boldsymbol{k}_p = (k_x, k_y, k_{p_z})$ due to planar symmetry (3.21), for some complex number k_{p_z}, and we used $k^2 - k_p^2 = k_z^2 - k_{p_z}^2$.

7.2 Average reflection

The average scattered wave is again given by (3.15), which by substituting the effective wave representation (4.1) and (5.10) leads to

$$\langle u_{\mathrm{sc}}(\boldsymbol{r})\rangle = \sum_{n,p}\int_{\mathcal{S}} \mathfrak{n}(\lambda_1)F_{p,n}(\lambda_1)\int_{\mathcal{R}_1} \mathrm{e}^{\mathrm{i}\boldsymbol{k}_p\cdot\boldsymbol{r}_1}\mathrm{u}_n(k\boldsymbol{r}-k\boldsymbol{r}_1)\mathrm{d}\boldsymbol{r}_1\mathrm{d}\lambda_1, \quad \text{for} \quad z < Z_1. \tag{7.4}$$

By using Green's second identity we can reduce the integral over $\mathcal{R}_1$ as done in (7.2). As the plate is thicker than any one particle, we then have that $Z_2 - a_1 - z > 0$ and $Z_1 + a_1 - z > 0$ for $z < Z_1$, which allows us to pick the positive argument in (F.5), evaluate (7.2), and reduce (7.4) to

$$\langle u_{\mathrm{sc}}(\boldsymbol{r})\rangle = R_{\text{plate}}\mathrm{e}^{\mathrm{i}\boldsymbol{k}_{\mathrm{ref}}\cdot\boldsymbol{x}}, \qquad \text{(average reflected field)} \tag{7.5}$$

where R_{plate} is the reflection coefficient:

$$R_{\text{plate}} = \sum_{n,p}\frac{2\pi\mathrm{i}^{\ell-1}}{k_z+k_{p_z}}\frac{\mathrm{Y}_n(\hat{\boldsymbol{k}}_{\mathrm{ref}})}{kk_z}\int_{\mathcal{S}} \mathfrak{n}(\lambda_1)F_{p,n}(\lambda_1)\left[\mathrm{e}^{\mathrm{i}(k_{p_z}+k_z)(Z_2-a_1)} - \mathrm{e}^{\mathrm{i}(k_{p_z}+k_z)(Z_1+a_1)}\right]\mathrm{d}\lambda_1, \tag{7.6}$$

we define $\boldsymbol{k}_{\mathrm{ref}} = (k_x, k_y, -k_z)$, used $\boldsymbol{k}_p = (k_x, k_y, k_{p_z})$ due to planar symmetry (3.21), and that $k^2 - k_p^2 = k_z^2 - k_{p_z}^2$.

For homogeneous materials, energy conservation is often presented in the form $1|R_{\text{plate}}|^2 + |cT_{\text{plate}}|^2$ for some constant c which depends on the material properties. In our case we do not expect such an identity to hold, because quadratic quantities are not preserved when taking an ensemble average [20, 48].

7.3 The average boundary conditions

When using only one effective wavenumber k_1 the equation (4.8) can be used to fully determine the field (5.10), like a boundary condition. Note we can use planar symmetry (3.20) and the form (5.10) because both the incident wave and material region share a planar symmetry.

The first step is to simplify (4.4):

$$\mathcal{I}_{p,n'n}(\boldsymbol{r}_1) = F_{p,n'}(\lambda_2)\int_{z_2=Z_2-a_2} \mathcal{U}_{n'n}(k\boldsymbol{r}_1 - k\boldsymbol{r}_2)\frac{\partial \mathrm{e}^{\mathrm{i}\boldsymbol{k}_p\cdot\boldsymbol{r}_2}}{\partial z_2} - \frac{\partial \mathcal{U}_{n'n}(k\boldsymbol{r}_1 - k\boldsymbol{r}_2)}{\partial z_2}\mathrm{e}^{\mathrm{i}\boldsymbol{k}_p\cdot\boldsymbol{r}_2}\,\mathrm{d}x_2\,\mathrm{d}y_2$$
$$- F_{p,n'}(\lambda_2)\int_{z_2=Z_1+a_2} \mathcal{U}_{n'n}(k\boldsymbol{r}_1 - k\boldsymbol{r}_2)\frac{\partial \mathrm{e}^{\mathrm{i}\boldsymbol{k}_p\cdot\boldsymbol{r}_2}}{\partial z_2} - \frac{\partial \mathcal{U}_{n'n}(k\boldsymbol{r}_1 - k\boldsymbol{r}_2)}{\partial z_2}\mathrm{e}^{\mathrm{i}\boldsymbol{k}_p\cdot\boldsymbol{r}_2}\,\mathrm{d}x_2\,\mathrm{d}y_2, \quad \boldsymbol{r}_1\in\mathcal{R}_1(a_{12}) \tag{7.7}$$

To explicitly calculate the above integrals, we use the translation matrices in Appendix B, followed by changing the integration variable to $\boldsymbol{r} = \boldsymbol{r}_2 - \boldsymbol{r}_1$ and then using the definition (F.1) to obtain

$$\mathcal{I}_{p,n'n}(\boldsymbol{r}_1) = F_{p,n'}(\lambda_2)\mathrm{e}^{\mathrm{i}\boldsymbol{k}_p\cdot\boldsymbol{r}_1}\sum_{n_1}(-1)^{\ell_1}c_{n'nn_1}\left[L_{n_1}(Z_2-a_2-z_1) - L_{n_1}(Z_1+a_2-z_1)\right], \tag{7.8}$$

where factor $(-1)^{\ell_1}$ appeared when substituting $\mathrm{u}_{n_1}(k\boldsymbol{r}_1 - k\boldsymbol{r}_2) = (-1)^{\ell_1}\mathrm{u}_{n_1}(k\boldsymbol{r}_2 - k\boldsymbol{r}_1)$ in the integrals.

We can use the formula (F.6) to easily calculate L_{n_1} by noting that $Z_2 - a_2 - z_1 > 0$ and $Z_1 + a_2 - z_1 < 0$. These inequalities are a result of $\boldsymbol{r}_1\in\mathcal{R}_1(a_{12})$ which implies that $Z_1 + a_1 + a_{12} \le z_1 \le Z_2 - a_1 - a_{12}$. Substituting (F.6) into (7.8) then leads to

$$\mathcal{I}_{p,n'n}(\boldsymbol{r}_1) = F_{p,n'}(\lambda_2)\mathrm{e}^{\mathrm{i}\boldsymbol{k}_p\cdot\boldsymbol{r}_1}\sum_{n_1}\mathrm{i}^{\ell_1}c_{n_1(\ell,-m)n'}\mathrm{Y}_{n_1}(\hat{\boldsymbol{k}})\times$$
$$\frac{2\pi\mathrm{i}}{kk_z}(-1)^{\ell+m}\left[(-1)^{m'-m}(k_{p_z}-k_z)\mathrm{e}^{\mathrm{i}(k_{p_z}+k_z)(Z_2-a_2-z_1)} - (-1)^{\ell'+\ell}(k_{p_z}+k_z)\mathrm{e}^{\mathrm{i}(k_{p_z}-k_z)(Z_1+a_2-z_1)}\right], \tag{7.9}$$

where we replaced $(-1)^{m_1} = (-1)^{m'-m}$, $(-1)^{\ell_1} = (-1)^{\ell'+\ell}$, and $c_{n'nn_1} = (-1)^{\ell+m}c_{n_1(\ell,-m)n'}$ by using the properties of $c_{n'nn_1}$ shown in Appendix B. These replacements allow us to simplify (7.9) by applying the contraction rule (B.12) and some rearrangement to reach:

$$\mathcal{I}_{p,n'n}(\boldsymbol{r}_1) = 4\pi\mathrm{i}^{\ell}\mathrm{Y}_{(\ell,-m)}(\hat{\boldsymbol{k}})\left[(-1)^{\ell}I_2\mathrm{e}^{\mathrm{i}(k_x,k_y,-k_z)\cdot\boldsymbol{r}_1} + (-1)^m I_1\mathrm{e}^{\mathrm{i}\boldsymbol{k}\cdot\boldsymbol{r}_1}\right], \tag{7.10}$$

where

$$\begin{cases} I_1 = -F_{p,n'}(\lambda_2)\mathrm{Y}_{n'}(\hat{\boldsymbol{k}})\mathrm{i}^{\ell'}\dfrac{2\pi\mathrm{i}}{kk_z}(-1)^{\ell'}(k_{p_z}+k_z)\mathrm{e}^{\mathrm{i}(k_{p_z}-k_z)(Z_1+a_2)}, \\ I_2 = F_{p,n'}(\lambda_2)\mathrm{Y}_{n'}(\hat{\boldsymbol{k}})\mathrm{i}^{\ell'}\dfrac{2\pi\mathrm{i}}{kk_z}(-1)^{m'}(k_{p_z}-k_z)\mathrm{e}^{\mathrm{i}(k_{p_z}+k_z)(Z_2-a_2)}, \end{cases} \tag{7.11}$$

and we also used $k_{p_x} = k_x$ and $k_{p_y} = k_y$. Substituting the above into (4.8) leads to

$$(-1)^m\mathrm{e}^{\mathrm{i}\boldsymbol{k}\cdot\boldsymbol{r}_1}\left[1 + \sum_{n'p}\int_{\mathcal{S}}\frac{I_1\bar{\mathfrak{n}}(\lambda_2)}{k^2-k_p^2}\mathrm{d}\lambda_2\right] + \mathrm{e}^{\mathrm{i}(k_x,k_y,-k_z)\cdot\boldsymbol{r}_1}(-1)^{\ell}\sum_{n'p}\int_{\mathcal{S}}\frac{I_2\bar{\mathfrak{n}}(\lambda_2)}{k^2-k_p^2}\mathrm{d}\lambda_2 = 0, \tag{7.12}$$

where we used that

$$\sum_{n'}\mathcal{V}_{n'n}(k\boldsymbol{r}_1)g_{n'} = 4\pi\mathrm{i}^{\ell}(-1)^m\mathrm{e}^{\mathrm{i}\boldsymbol{k}\cdot\boldsymbol{r}_1}\mathrm{Y}_{\ell-m}(\hat{\boldsymbol{k}}),$$

which holds for incident plane waves with the coefficients (2.5) and can be shown by using (A.2) and the contraction rule (B.12).

For (7.12) to hold for every $\boldsymbol{r}_1\in\mathcal{R}_1(a_{12})$ leads to two equations: one for the term multiplying $\mathrm{e}^{\mathrm{i}(k_x,k_y,-k_z)\cdot\boldsymbol{r}_1}$ and another for the terms multiplying $\mathrm{e}^{\mathrm{i}\boldsymbol{k}\cdot\boldsymbol{r}_1}$. These two equations can be written in the form:

$$1 + \sum_{n'p}\int_{\mathcal{S}}\frac{I_1\bar{\mathfrak{n}}(\lambda_2)}{k^2-k_p^2}\mathrm{d}\lambda_2 = 0, \qquad \text{(surface } Z_1\text{)} \tag{7.13}$$

$$\sum_{n'p}\int_{\mathcal{S}}\frac{I_2\bar{\mathfrak{n}}(\lambda_2)}{k^2-k_p^2}\mathrm{d}\lambda_2 = 0, \qquad \text{(surface } Z_2\text{)} \tag{7.14}$$

where I_1 and I_2 are given in (7.11).

For a finite plate, both (7.13) and (7.14) need to be enforced to restrict the $F_{p,n}(\lambda_1)$. If the sum over p has only two terms, using one a forward propagating and the other a backward propagating mode, then these equations can be used to obtain a unique solution for the $F_{p,n}$. This typically occurs when using only one effective wavenumber k_1. For reflection from a halfspace, only (7.13) should be enforced, which is a generalisation of the three dimensional version of [44, Equation (20)].

8 Numerical results: plane-wave incident on a particulate sphere

This paper is the first, to our knowledge, to provide analytic solutions for the average wave scattered from particles within a spherical region $\mathcal{R}$ as given by (6.3) and (6.7). The methods used previously[41, 51] have approximated the scattered field by assuming that the ensemble averaged sphere behaves like a homogeneous sphere occupying the region $\mathcal{R}$ with some effective properties. For these reasons, in this section we numerically compare these approaches.

Results presented below are implemented and tested in [29], with an example given in manual/sphere.

For all the results below, we avoid combining a high particle volume fraction with a high frequency, as this regime triggers multiple wavenumbers with low imaginary parts, as shown in Figure 4. Whereas the calculations below rely on equation (6.3) giving a unique solution, which only occurs when using just one effective wavenumber. Using only one wavenumber is an excellent approximation when its imaginary part is much smaller than all the other wavenumbers, as shown in Figure 5. See [25, 26] for details on how to calculate reflection and transmission when multiple effective wavenumbers have a small imaginary part.

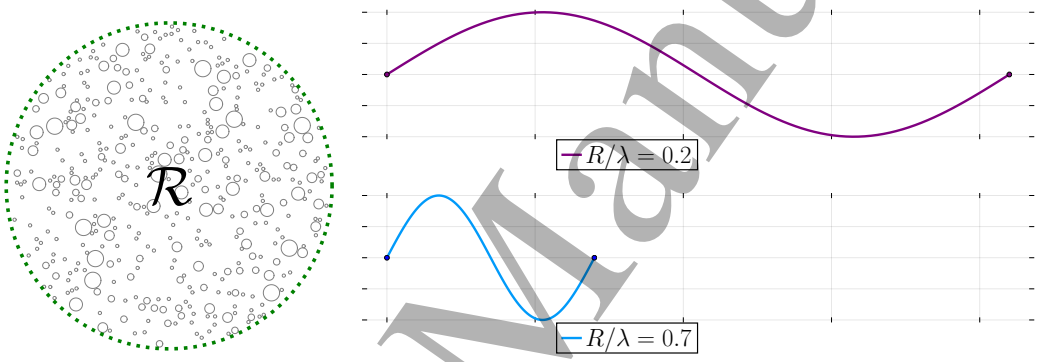

Figure 6: An illustration of the size of the spherical region $\mathcal{R}$, the size of particles inside, and the typical length of the incident wavelengths λ used for the results in Figures 7 - 9. Note that R is the radius of $\mathcal{R}$, and numerical parameters used in this section are in Table 2.

	mass density	wave speed	radius	volume %
Solid particles	$\rho_s/\rho = 10$	$c_s/c = 10$	$a_s/R = 1/20$	$\varphi_s = 15\%$
Void particles	$\rho_v/\rho = 0.1$	$c_v/c = 0.1$	$a_v/R = 1/20$	$\varphi_v = 5\%$

Table 2: Material properties used for the numerical experiments. Note that R is the radius of the spherical region $\mathcal{R}$.

The analytic scattered field. For each (angular) frequency ω, we calculate the effective wavenumber k_1 with the smallest imaginary part. We then follow Algorithm 4 and Algorithm 6 to calculate the scattered field. As a reminder, this method does not assume the spherical region behaves like some homogeneous sphere; instead these results are from careful homogenisation of all the scattered waves.

Two different homogeneous spheres. We can approximately calculate the scattered wave from the sphere $\mathcal{R}$ by assuming that $\mathcal{R}$ is filled with some homogeneous material. Below, we choose two different ways to approximate the density and sound speed of this homogeneous material we use to fill $\mathcal{R}$. Note that there are many possible chooses for the density and sound speed and no clear "best choice".

1. **Hom. Low Freq.**: we assume the sphere has the effective density ρ_* and effective bulk module β_* given by (5.23), which results in the sound speed $c_* = \sqrt{\beta_*/\rho_*}$.

2. **Hom. Complex k_1**: we assume the sphere has the same complex wavenumber k_1 used for the analytic solution, which then implies it has sound speed $c_1 = \omega/k_1$. For the effective density, we again choose ρ_* given by (5.23).

After choosing one of these approximations, we can calculate the scattering coefficients F_n by using the T-matrix (2.8). Taking the origin to be the centre of the spherical region $\mathcal{R}$, we can then express the scattered field in the form

$$(\text{scattered field}) = \sum_n F_n \mathrm{u}_n(k\boldsymbol{r}), \quad r > R,$$

for a sphere of radius R. For the analytic solution we have $F_n = \int_{\mathcal{S}} \mathfrak{F}_n(\lambda_1)\mathfrak{n}(\lambda_1)d\lambda_1$ from (6.7), and for the numerical results we approximate the integral as a sum.

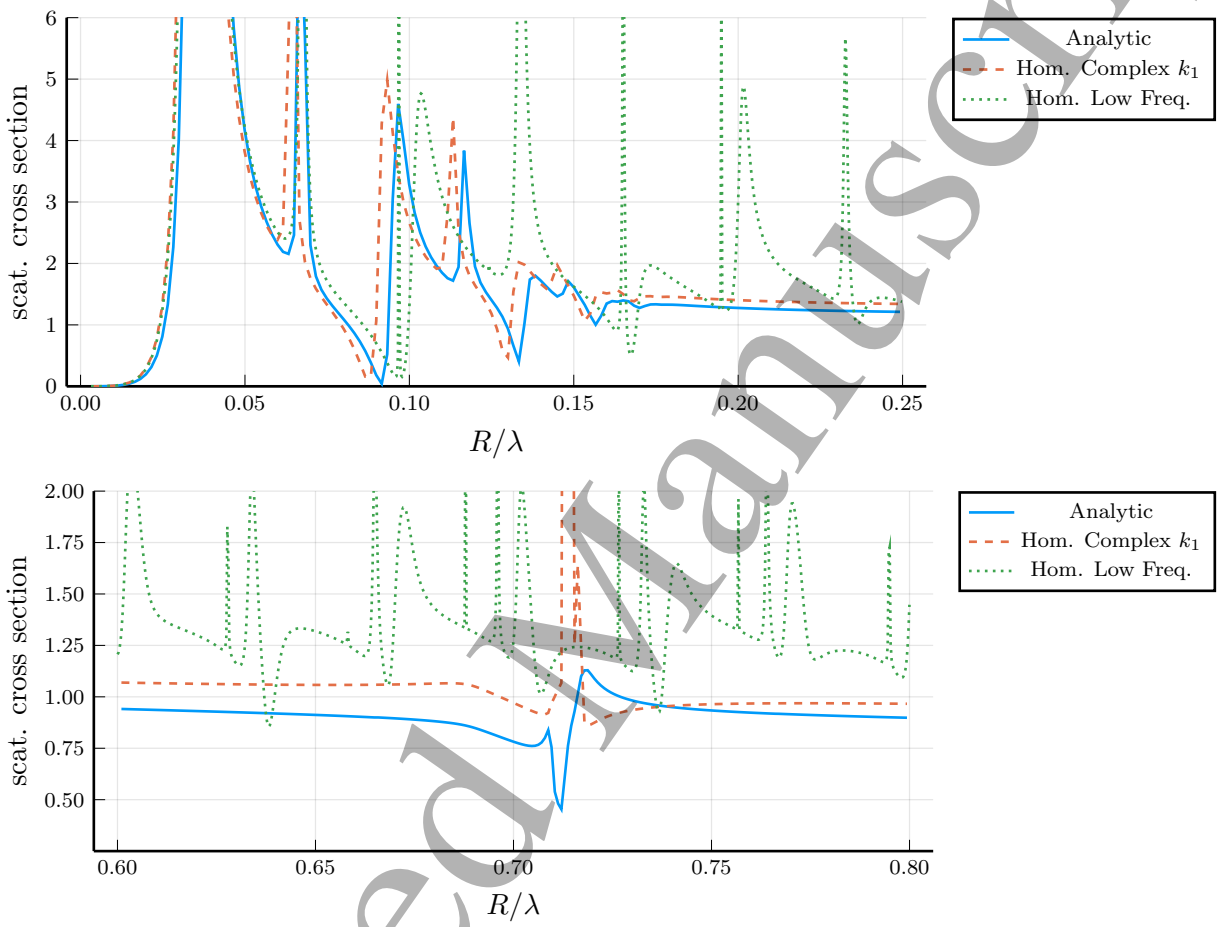

Figure 7: Shows the scattering cross-section of the average scattered field from a sphere filled with particles. The three different methods used are described in the beginning of this section, and the properties used are given in Table 2. The Hom. Complex k_1 exhibits a strong resonance, with the peak climbing above 13, which is not shown to avoid zooming out too far. At a similar frequency, the Analytic solution exhibits the opposite, where scattering is very weak. Note we did not show the range $0.25 < R/\lambda < 0.6$ as it is less interesting.

Frequency sweep. We begin with a frequency sweep and use the particle properties given in Table 2. For each frequency, we calculate the scattering cross section for the three methods described above: the analytic and the two homogeneous spheres. The results are shown in Figure 7.

We define the non-dimensional scattering cross section by [60]

$$(\text{scat. cross section}) = \frac{1}{2\pi(kR)^2} \sum_n |F_n|^2,$$

where the $|\cdot|$ represents the absolute value. The above is dimensionless and the natural way to compare with the geometrical cross section of the sphere [36]. In the standard notation, σ_s often denotes the scattering cross section, in which case our non-dimensional scattering cross section is equal to $\sigma_s/(2\pi R^2)$.

As expected the three methods converge for low frequencies, as shown in Figure 7. For $R/\lambda > 0.05$ the Homogeneous Low Frequency sphere quickly diverges from the other two solutions, and then has far more resonant frequencies. The two methods that use the same effective wavenumber, k_1, stay closer together, but are significantly different even before reaching $R/\lambda = 0.6$. Around $R/\lambda = 0.72$ we see that both the analytic and the Homogeneous Complex k_1 methods hit a resonant frequency, but display very different responses. To further investigate this, we plot the full scattered field for the three methods in Figure 8. These fields show contour maps for the slice $y = 0$. The main difference between the methods is that the analytic solution has a weaker scattered field and also has a smaller shadow region.

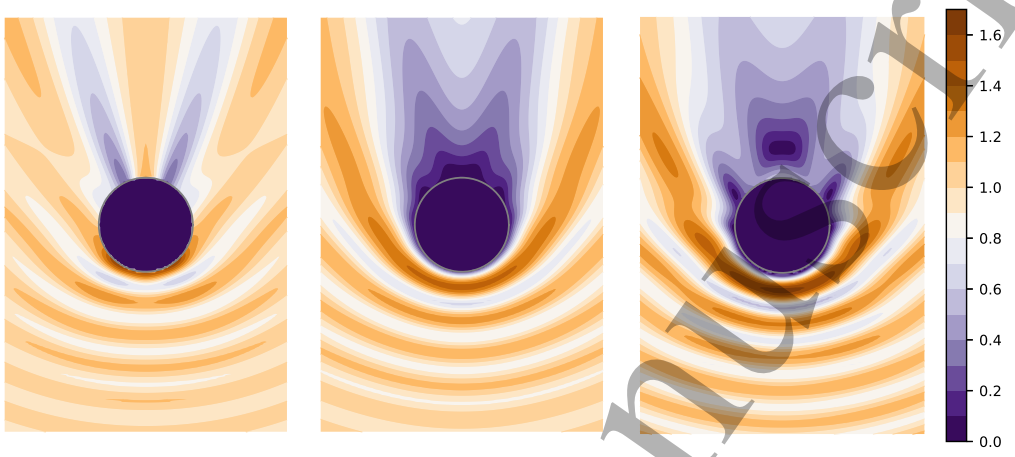

Figure 8: Comparing the absolute value of the scattered field of the three methods (from left to right): analytic, hom. complex k_1, and hom. low freq. for $R/\lambda = 0.71$. Figure 7 shows the scattering cross-section for these three methods over a large frequency range. Code to reproduce this figure is given in manual/sphere.

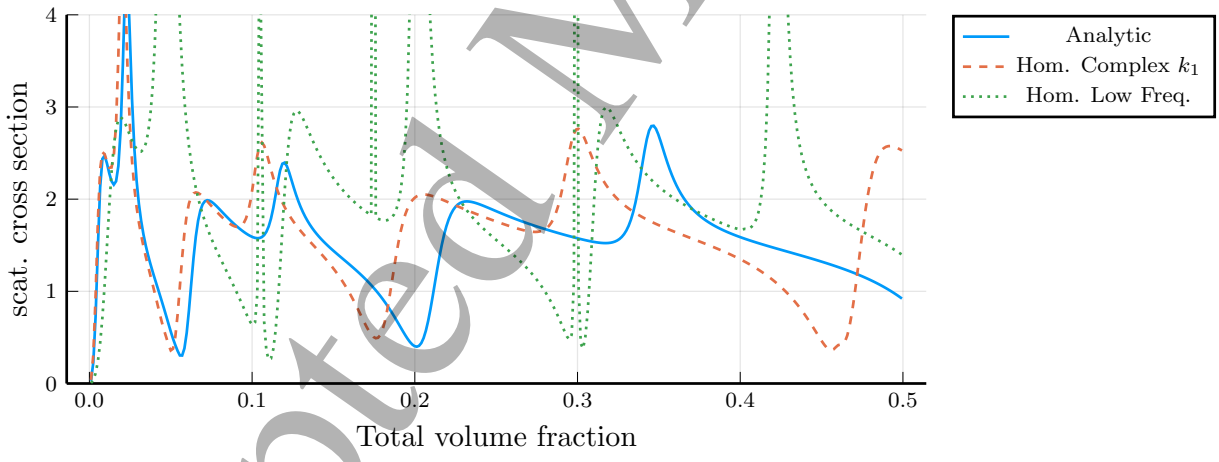

Figure 9: For a fixed frequency which corresponds to $R/\lambda = 0.133$, chosen as it is a lowish frequency, see into, and it is a local min. in Figure 7.

Varying the particle volume fraction. The effects of multiple scattering between particles vary significantly with the volume fraction of the particles as shown in Figure 9. To produce these results we used a fixed frequency which corresponds to $R/\lambda = 0.133$. This frequency was chosen as it is relatively low and is the local minimum of the analytic scattering cross-section in Figure 7. As this is a relatively low frequency, it avoids the need to use multiple effective wavenumbers even for large volume fraction, as described in the beginning of this section.

For a moderate volume fraction, Hom. Complex k_1 is qualitatively a good approximation (except close to resonant frequencies) as shown in Figure 7. However, when increasing the volume fraction we see a clear drift between Hom. Complex k_1 and the Analytic method in Figure 9. Again we notice that Hom. Low Freq. has more resonant frequencies, and they are more extreme.

9 Discussion

Much has already been understood about a plate, or half-space, filled with a random mix of particles, including how to calculate, and make sense of, the effective wavenumbers, reflection, and transmission [62, 61, 8, 26, 25, 38, 56, 48]. These results are now used to probe emulsions, colloids, and slurry [9, 1] with sound, and planetary systems with light [48], among other applications.

A question that remained was: how to make sense of other regions $\mathcal{R}$ not shaped like a plate? For example, like a droplet filled with a particulate.

Effective wavenumbers. One milestone of this paper was to show that any region $\mathcal{R}$ filled with the same particulate material will have the same effective wavenumbers, and these effective wavenumbers are given by solving (5.15) or (5.16), with the low frequency properties given by (5.23). In fact, (5.16) is simpler to solve than the dispersion equations previously presented in the literature.

A key step we used was to represent the average wave as a sum of wave potentials each with a different effective wavenumber, as shown by (4.1). How useful this representation is depends on how fast the sum converges. For plane waves this sum was shown to converge rapidly [26, 25] and depend on how the effective wavenumbers are distributed in the complex plane. As the wavenumbers do not depend on the geometry, this rapid convergence is likely to carry over to other geometries.

Multiple effective wavenumbers. In this work, we concentrated on scenarios where all the effective wavenumbers, except one, lead to wave modes which decay rapidly. That is, we make use of only one effective wavenumber. This scenario, which occurs for most frequencies and particle properties simplifies the equations. See [26] for an example where many effective wavenumbers are used. It remains an open challenge to find a simpler way to incorporate all effective wavenumbers for scenarios such as a sphere filled with particles.

The ensemble wave equation. Our results have enabled us to take effective wavenumbers from a halfspace, or a plate, and use them to calculate the average scattered wave from a sphere filled with particles. To our knowledge, we are the first to provide a clear first-principals approach to achieve this. Beyond the examples we present in this paper, like a sphere filled with particles, our ensemble wave equation (4.7) and ensemble boundary conditions (4.8) can be used to calculate the average field for regions of any shape. Though, depending on the shape, this may require considerable work.

Numerical results. To both demonstrate that our method can completely describe the average scattered field, and to compare with previous approaches, we present some numerical results for a sphere filled with particles in Section 8. We compared our method with approaches which assume the region $\mathcal{R}$ is made of some homogeneous material with effective properties. As expected, the different methods converge for low-frequency, as shown in Figures 7 and 9, though there are significant differences for finite frequencies. For one specific frequency, the difference between the methods is illustrated by a field plot in Figure 8.

Validation. The next natural step is to validate our models. Numerical validation would be ideal, as there are robust numerical methods for multiple scattering [30, 24, 48, 41]. Numerical methods can also clarify the assumptions used in the modelling, such as the choice of pair-correlation and the quasi-crystalline approximation. However, a major issue, that has prevented substantial validation, is that these numerical methods have struggled to simulate an infinite halfspace or infinite plate required by most of the available theoretical predictions [27, 11, 10].

Now, with our framework, numerical validation for finite sized sphere filled with particles should be straight-forward. This will allow a clear way to verify the statistical assumptions used, and the range of their validity.

Electromagnetism and Elastodynamics. Our framework deals with the scalar wave equation. There exist in the literature clear routes on how to extend effective wave theory from the scalar version to elastodynamics [12], thermo-visco-elasticity [40, 54] and electromagnetism [55, 16, 15], though each requires extra algebraic manipulation. In light scattering, it is far easier to measure the average of the scattered intensity [48], though it requires the average of the scattered field, which is what we calculate in this work. Extending our framework to calculate the average intensity should enable accurate models for scattering from spheres and other compact objects.

10 Code and reproducibility

The examples and theory we develop above has been implemented in the publicly available package EffectiveWaves.jl [29] written in Julia [4, 5]. All calculations presented have been rigorously unit tested. To calculate wavenumbers is in shown in manual/wavenumbers, with an example on how difference symmetries lead to the same wavenumbers in examples/equivalent-symmetries. Finally, some of the calculations from Section 6 on scattering from a sphere are shown in manual/sphere.

11 Acknowledgements

Gerhard wishes to gratefully thank the UK Acoustic Network funded by EPSRC (EP/R005001/1) for a generous travel support which made it possible for Gerhard to visit Sheffield in the fall 2019. The authors would also like to acknowledge the late Michael Mishchenko for putting the authors in touch, which ultimately led to this paper, and for his amazing contribution to the field of scattering. The authors are also thankful to Thomas Wriedt for organising the Bremen Workshop on Light Scattering.

A Spherical harmonics

The associated Legendre functions, defined for non-negative integers $\ell \geq m \geq 0$, are denoted $\mathrm{P}_\ell^m(x)$, and defined by

$$\mathrm{P}_\ell^m(x) = (1-x^2)^{m/2}\frac{\mathrm{d}^m}{\mathrm{d}x^m}\mathrm{P}_\ell(x), \quad x \in [-1,1],$$

where $\mathrm{P}_\ell(x)$ is the Legendre polynomials. For a negative integer value of m, we use ($m = -1, -2, \ldots$)

$$\mathrm{P}_\ell^m(x) = (-1)^{|m|}\frac{(\ell-|m|)!}{(\ell+|m|)!}\mathrm{P}_\ell^{|m|}(x), \quad x \in [-1,1].$$

The spherical harmonics are denoted $\mathrm{Y}_{\ell m}(\theta,\phi)$ and they are defined by [17, (2.5.29), p. 24]

$$\mathrm{Y}_n(\hat{\boldsymbol{r}}) = \mathrm{Y}_{\ell m}(\theta,\phi) = (-1)^m\sqrt{\frac{2\ell+1}{4\pi}\frac{(\ell-m)!}{(\ell+m)!}}\mathrm{P}_\ell^m(\cos\theta)\mathrm{e}^{\mathrm{i}m\phi}, \tag{A.1}$$

where we committed a small abuse in notation as $\hat{\boldsymbol{r}} = (\cos\phi\sin\theta, \sin\phi\sin\theta, \cos\theta)$, where the angles θ and ϕ can be complex. The indices ℓ and m take the following values:

$$m = -\ell, -\ell+1, \ldots, -1, 0, 1, \ldots, \ell, \quad \ell = 0, 1, 2, \ldots.$$

For the special case $\hat{\boldsymbol{k}} = \hat{\boldsymbol{z}}$ we have that

$$4\pi\mathrm{Y}_n^*(\hat{\boldsymbol{z}}) = \delta_{m,0}\sqrt{4\pi(2\ell+1)}.$$

The spherical harmonics satisfy the parity relation and complex conjugate

$$\mathrm{Y}_n(-\hat{\boldsymbol{r}}) = (-1)^\ell\mathrm{Y}_n(\hat{\boldsymbol{r}}), \qquad \mathrm{Y}_{\ell m}^*(\hat{\boldsymbol{r}}^*) = (-1)^m\mathrm{Y}_{\ell -m}(\hat{\boldsymbol{r}}),$$

and $\mathrm{Y}_n(\hat{\boldsymbol{r}})$ are orthonormal over the real unit sphere Ω, that is

$$\int_\Omega \mathrm{Y}_{\ell m}^*(\theta,\phi)\mathrm{Y}_{\ell' m'}(\theta,\phi)\sin\theta\ \mathrm{d}\theta\,\mathrm{d}\phi = (-1)^m\int_\Omega \mathrm{Y}_{\ell -m}(\theta,\phi)\mathrm{Y}_{\ell' m'}(\theta,\phi)\sin\theta\ \mathrm{d}\theta\,\mathrm{d}\phi = \delta_{\ell,\ell'}\delta_{m,m'}.$$

Plane waves can be expanded in terms of spherical harmonics by using:

$$\mathrm{e}^{\mathrm{i}\boldsymbol{x}\cdot\boldsymbol{y}} = 4\pi\sum_{n_1}\mathrm{i}^{\ell_1}(-1)^{m_1}j_{\ell_1}(xy)\mathrm{Y}_{n_1}(\hat{\boldsymbol{x}})\mathrm{Y}_{\ell_1-m_1}(\hat{\boldsymbol{y}}) = 4\pi\sum_{n_1}\mathrm{i}^{\ell_1}(-1)^{m_1}\mathrm{v}_{n_1}(y\boldsymbol{x})\mathrm{Y}_{\ell_1-m_1}(\hat{\boldsymbol{y}}) \tag{A.2}$$

where both $\boldsymbol{x}$ and $\boldsymbol{y}$ can be complex vectors, and we use the dot product to mean $(x_1,x_2,x_3)\cdot(y_1,y_2,y_3) = x_1y_1 + x_2y_2 + x_3y_3$ with no conjugation.

B Translation matrices

The translation properties of the spherical waves are instrumental for the formulation and the solution of the scattering problem of many individual particles. These translation properties are well know, and we refer to, *e.g.*, [6, 21] for details. Some of their properties are reviewed in this appendix and a simple proof of these matrices are given in the supplementary material.

Let $\boldsymbol{r}' = \boldsymbol{r} + \boldsymbol{d}$, then the translation matrices for a translation $\boldsymbol{d}$ are [6]

$$\begin{cases} \mathrm{v}_n(k\boldsymbol{r}') = \sum_{n'} \mathcal{V}_{nn'}(k\boldsymbol{d})\mathrm{v}_{n'}(k\boldsymbol{r}), & \text{for all } \boldsymbol{d} \\ \mathrm{u}_n(k\boldsymbol{r}') = \sum_{n'} \mathcal{V}_{nn'}(k\boldsymbol{d})\mathrm{u}_{n'}(k\boldsymbol{r}), & |\boldsymbol{r}| > |\boldsymbol{d}| \\ \mathrm{u}_n(k\boldsymbol{r}') = \sum_{n'} \mathcal{U}_{nn'}(k\boldsymbol{d})\mathrm{v}_{n'}(k\boldsymbol{r}), & |\boldsymbol{r}| < |\boldsymbol{d}| \end{cases}. \tag{B.1}$$

Translation in the opposite direction is identical to the Hermitian conjugate of the translation matrices [53], *i.e.*,

$$\mathcal{V}_{nn'}(-k\boldsymbol{d}) = \mathcal{V}^*_{n'n}(k^*\boldsymbol{d}) = (-1)^{\ell-\ell'}\mathcal{V}_{nn'}(k\boldsymbol{d}), \quad \mathcal{U}_{nn'}(-k\boldsymbol{d}) = (-1)^{\ell-\ell'}\mathcal{U}_{nn'}(k\boldsymbol{d}). \tag{B.2}$$

The translation matrix $\mathcal{V}_{nn'}(k\boldsymbol{d})$ is identical to $\mathcal{U}_{nn'}(k\boldsymbol{d})$ but with $\mathrm{h}^{(1)}_\lambda(k|\boldsymbol{d}|)$ replaced with $\mathrm{j}_\lambda(k|\boldsymbol{d}|)$.

Notice that the translation matrices $\mathcal{V}_{nn'}(k\boldsymbol{d})$ and $\mathcal{U}_{nn'}(k\boldsymbol{d})$ have the form

$$\mathcal{V}_{nn'}(k\boldsymbol{d}) = \sum_{n_1} c_{nn'n_1}\mathrm{v}_{n_1}(k\boldsymbol{d}), \quad \mathcal{U}_{nn'}(k\boldsymbol{d}) = \sum_{n_1} c_{nn'n_1}\mathrm{u}_{n_1}(k\boldsymbol{d}). \tag{B.3}$$

where the summation over the multi-index $n_1 = \{\ell_1, m_1\}$ effectively is over $|\ell - \ell'| \leq \ell_1 \leq \ell + \ell'$, and $m_1 = m - m'$. The explicit values of the coefficients $c_{nn'n_1}$ are, see the supplementary material

$$c_{nn'n_1} = 4\pi \mathrm{i}^{\ell'-\ell+\ell_1} \int_\Omega \mathrm{Y}_n(\theta,\phi)\mathrm{Y}^*_{n'}(\theta,\phi)\mathrm{Y}^*_{n_1}(\theta,\phi)\,\sin\theta\,\mathrm{d}\theta\,\mathrm{d}\phi. \tag{B.4}$$

which can be expressed with the Wigner 3-j symbol [17, (4.6.3), p. 63] in the form

$$c_{nn'n''} = \mathrm{i}^{\ell'-\ell+\ell''}(-1)^m\sqrt{4\pi(2\ell+1)(2\ell'+1)(2\ell''+1)}\begin{pmatrix}\ell & \ell' & \ell'' \\ 0 & 0 & 0\end{pmatrix}\begin{pmatrix}\ell & \ell' & \ell'' \\ m & -m' & -m''\end{pmatrix}. \tag{B.5}$$

Note that the coefficients $c_{nn'n''}$ are all real due to orthogonality in the azimuthal index. Further the $c_{nn'n''}$ are only non-zero when

$$m - m' = m'', \quad |\ell - \ell'| \leq \ell'' \leq \ell + \ell', \quad \ell + \ell' + \ell'' = \text{even integer}, \tag{B.6}$$

and should only be evaluated for $\ell, \ell', \ell'' \geq 0$ and

$$-\ell \leq m \leq \ell, \quad -\ell' \leq m' \leq \ell', \quad -\ell'' \leq m'' \leq \ell''. \tag{B.7}$$

Other often used notation is the Gaunt coefficient [45]:

$$4\pi\mathcal{G}(\ell, m; \ell' m'; \ell_1) = \mathrm{i}^{-\ell'+\ell-\ell_1}(-1)^{m'}c_{(\ell,m)(\ell',-m')(\ell_1,m+m')}, \tag{B.8}$$

and the Clebsch-Gordan coefficients

$$c_{nn'n''} = \mathrm{i}^{\ell'-\ell+\ell''}(-1)^{m'}\sqrt{4\pi\frac{(2\ell+1)(2\ell'+1)}{(2\ell''+1)}}\langle \ell\, 0\, \ell'\, 0|\ell''\, 0\rangle\langle \ell\, m\, \ell'\, -m'|\ell''\, m''\rangle. \tag{B.9}$$

The special case $c_{nn(0,0)} = \sqrt{4\pi}$ and following properties are useful:

$$c_{nn'n''} = c_{nn''n'} = c_{(\ell,-m)(\ell',-m')(\ell'',-m'')}, \tag{B.10}$$

$$c_{nn'n''} = (-1)^{m''+\ell''}c_{n'n(\ell'',-m'')} = (-1)^{\ell'+m'}c_{n''(\ell',-m')n}, \tag{B.11}$$

$$\sum_{n_1}\mathrm{i}^{\ell_1}\mathrm{Y}_{n_1}(\theta,\phi)c_{n_1n'n} = 4\pi\mathrm{i}^{\ell+\ell'}\mathrm{Y}_n(\theta,\phi)\mathrm{Y}_{n'}(\theta,\phi), \tag{B.12}$$

where the last is the contraction rule, or the linearisation formula [45]. For real θ and ϕ the linearisation formula can be deduced by multiplying both sides of (B.12) by $\mathrm{Y}^*_{n_2}(\hat{\boldsymbol{r}})$, then integrating over $\hat{\boldsymbol{r}}$, and applying the definition (B.4).

C Separating the effective waves in equation (4.6)

In this appendix, we address the solution of an equation of the form

$$\sum_{p=0}^{P} \psi_p(\boldsymbol{r}) = 0,$$

where the functions $\psi_p(\boldsymbol{r})$ satisfy

$$\nabla^2 \psi_p(\boldsymbol{r}) = -k_p^2 \psi_p(\boldsymbol{r}),$$

where $k_p \neq k_q$, $p \neq q$. The following theorem proves that the solution of this equation is $\psi_p(\boldsymbol{r}) = 0$, $p = 0, 1, 2, \ldots, P$:

Theorem C.1. *Let the functions $\psi_p(\boldsymbol{r})$ for $p = 0, 1, 2, \ldots, P$, satisfy $\nabla^2 \psi_p(\boldsymbol{r}) = \alpha_p \psi_p(\boldsymbol{r})$ for $\boldsymbol{r} \in \mathcal{R}$. Assuming $\alpha_p \neq \alpha_q$ for every $p \neq q$, then the only solution to*

$$\sum_{p=0}^{P} \psi_p(\boldsymbol{r}) = 0, \quad \textit{for all } \ \boldsymbol{r} \in \mathcal{R}, \tag{C.1}$$

is $\psi_p(\boldsymbol{r}) = 0$ for $p = 0, 1, 2, \ldots, P$.

Proof. From the assumption in the theorem, we have

$$\nabla^2 \sum_{p=0}^{P} \psi_p(\boldsymbol{r}) = \sum_{p=0}^{P} \alpha_p \psi_p(\boldsymbol{r}) = 0,$$

for any open ball within $\mathcal{R}$. Or, more generally, by repeated use of the Laplace operator

$$\sum_{p=0}^{P} \alpha_p^n \psi_p(\boldsymbol{r}) = 0, \quad \text{for } \ n = 0, 1, 2, \ldots, P,$$

which we summarise in a matrix notation

$$\begin{pmatrix} 1 & 1 & 1 & \cdots & 1 \\ \alpha_0 & \alpha_1 & \alpha_2 & \cdots & \alpha_P \\ \alpha_0^2 & \alpha_1^2 & \alpha_2^2 & \cdots & \alpha_P^2 \\ \alpha_0^3 & \alpha_1^3 & \alpha_2^3 & \cdots & \alpha_P^3 \\ \vdots & \vdots & \vdots & \ddots & \vdots \\ \alpha_0^P & \alpha_1^P & \alpha_2^P & \cdots & \alpha_P^P \end{pmatrix} \begin{pmatrix} \psi_0(\boldsymbol{r}) \\ \psi_1(\boldsymbol{r}) \\ \psi_2(\boldsymbol{r}) \\ \psi_3(\boldsymbol{r}) \\ \vdots \\ \psi_P(\boldsymbol{r}) \end{pmatrix} = \begin{pmatrix} 0 \\ 0 \\ 0 \\ 0 \\ \vdots \\ 0 \end{pmatrix}.$$

The matrix on the left-hand side is the transpose of the Vandermonde matrix with determinant $\prod_{0 \leq p < q \leq P} (\alpha_q - \alpha_p)$, see *e.g.*, [14]. Under the assumption $\alpha_p \neq \alpha_q$, $p \neq q = 0, 1, 2, \ldots, P$, this matrix determinant is non-zero, and we obtain the result of the theorem, $\psi_p(\boldsymbol{r}) = 0$ for $p = 0, 1, 2, \ldots, P$ and $\boldsymbol{r}$ within some open ball in $\mathcal{R}$. By analyticity of the solutions to the Helmholtz equation, the functions $\psi_p(\boldsymbol{r}) = 0$ for $p = 0, 1, 2, \ldots, P$ and $\boldsymbol{r} \in \mathcal{R}$. □

D The matrix G_{n,n_2}

Here, we calculate the dimensionless matrix $G_{n,n_2}(\lambda_1)$ by substituting the spherical basis expansion (5.1) into (4.5), which leads to

$$\mathcal{J}_{p,n'n}(\boldsymbol{r}_1) = \sum_{n_1 n_2} F_{p,n'n_1}(\lambda_2) \mathrm{v}_{n_2}(k_p \boldsymbol{r}_1) \int_{\partial B(\mathbf{0}; a_{12})} \left\{ \mathcal{U}_{n'n}(-k\boldsymbol{r}) \frac{\partial \mathcal{V}_{n_1 n_2}(k_p \boldsymbol{r})}{\partial \boldsymbol{\nu}} - \frac{\partial \mathcal{U}_{n'n}(-k\boldsymbol{r})}{\partial \boldsymbol{\nu}} \mathcal{V}_{n_1 n_2}(k_p \boldsymbol{r}) \right\} \mathrm{d}A,$$

From Appendix B, we have that

$$\mathcal{U}_{n'n}(-k\boldsymbol{r}) = (-1)^{\ell' - \ell} \sum_{n''} c_{n'nn''} \mathrm{u}_{n''}(k\boldsymbol{r}),$$

$$\mathcal{V}_{n_1 n_2}(k_p \boldsymbol{r}) = \sum_{n_3} c_{n_1 n_2 n_3} \mathrm{v}_{n_3}(k_p \boldsymbol{r}).$$

Integrating over the spherical surface $\partial B(\mathbf{0}; a_{12})$, and using the orthogonality of the spherical harmonics, we obtain

$$\mathcal{J}_{p,n'n}(\boldsymbol{r}_1) = -\sum_{n_1 n_2} F_{p,n'n_1}(\lambda_2) \mathrm{v}_{n_2}(k_p \boldsymbol{r}_1) \sum_{n_3} c_{nn'n_3} c_{n_1 n_2 n_3} a_{12} \mathrm{N}_{\ell_3}(k a_{12}, k_p a_{12}), \tag{D.1}$$

where $\mathrm{N}_\ell(x, z)$ is defined by (5.5). When substituting the above into (4.7) leads to the matrix $G_{n,n_2}(\lambda_1)$ defined by (5.4).

E Effective plane-waves

Here, we show that we recover the plane-wave dispersion equation deduced in much of the literature from our general ensemble wave equation (4.7). We use the plane-wave representation (5.10) together with (A.2) to write

$$f_{p,n'}(\boldsymbol{r}_1,\lambda_1) = F_{p,n'}(\lambda_1)\mathrm{e}^{\mathrm{i}\boldsymbol{k}_p\cdot\boldsymbol{r}_1} = 4\pi F_{p,n'}(\lambda_1)\sum_{n_1}\mathrm{i}^{\ell_1}\mathrm{j}_{\ell_1}(k_p r_1)Y^*_{n_1}(\hat{\boldsymbol{r}}_1)Y_{n_1}(\hat{\boldsymbol{k}}_p), \tag{E.1}$$

$$f_{p,n'}(\boldsymbol{r}_1+\boldsymbol{r},\lambda_2) = 4\pi f_{p,n'}(\boldsymbol{r}_1,\lambda_2)\sum_{n_1}\mathrm{i}^{\ell_1}\mathrm{j}_{\ell_1}(k_p r)Y^*_{n_1}(\hat{\boldsymbol{r}})Y_{n_1}(\hat{\boldsymbol{k}}_p), \tag{E.2}$$

where we used (5.12).

Using the above, we can simplify (4.7) by calculating:

$$\begin{aligned}\mathcal{J}_{p,n'n}(\boldsymbol{r}_1) &= f_{p,n'}(\boldsymbol{r}_1,\lambda_2)4\pi\sum_{n_1}\mathrm{i}^{\ell_1}Y_{n_1}(\hat{\boldsymbol{k}}_p)\int_{\partial B(\boldsymbol{0};a_{12})}Y^*_{n_1}(\hat{\boldsymbol{r}})\left(\mathcal{U}_{n'n}(-k\boldsymbol{r})\frac{\partial \mathrm{j}_{\ell_1}(k_p r)}{\partial r} - \frac{\partial \mathcal{U}_{n'n}(-k\boldsymbol{r})}{\partial r}\mathrm{j}_{\ell_1}(k_p r)\right)\mathrm{d}A\\ &= -f_{p,n'}(\boldsymbol{r}_1,\lambda_2)4\pi a_{12}(-1)^{\ell'-\ell}\sum_{n_1}\mathrm{i}^{\ell_1}Y_{n_1}(\hat{\boldsymbol{k}}_p)c_{n'nn_1}\mathrm{N}_{\ell_1}(ka_{12},k_p a_{12}),\end{aligned}$$

where we used $\mathcal{U}_{nn'}(-k\boldsymbol{d}) = (-1)^{l-l'}\mathcal{U}_{nn'}(k\boldsymbol{d})$ followed by $\mathcal{U}_{nn'}(k\boldsymbol{d}) = \sum_{n_1} c_{nn'n_1}\mathrm{u}_{n_1}(k\boldsymbol{d})$, and (5.5). Substituting the above into (4.7) then leads to the plane-wave eigensystem (5.11). The above dispersion equation is the same[8] as [38, equation (4.20)] (where you need to set $\mathcal{A}^m_n = 0$) when considering only one type of particle (no integer over $\mathcal{S}$), and only one effective wave.

F Integrals of spherical and plane waves

When dealing with effective plane-waves, we need to evaluate the following integral:

$$L_n(z) = \int_{\mathbb{R}^2}\mathrm{u}_n(k\boldsymbol{r})\frac{\partial \mathrm{e}^{\mathrm{i}\boldsymbol{k}_p\cdot\boldsymbol{r}}}{\partial z} - \frac{\partial \mathrm{u}_n(k\boldsymbol{r})}{\partial z}\mathrm{e}^{\mathrm{i}\boldsymbol{k}_p\cdot\boldsymbol{r}}\,\mathrm{d}x\,\mathrm{d}y. \tag{F.1}$$

These integrals converge when $\operatorname{Im} k \geq |\operatorname{Im} k_{p_x}| + |\operatorname{Im} k_{p_y}|$, where $\boldsymbol{k}_p = (k_{p_x}, k_{p_y}, k_{p_z})$. This inequality holds when using planar symmetry (3.21), which together with $\boldsymbol{k} = (k_x, k_y, k_z)$ implies that $k_{p_x} = k_x$ and $k_{p_y} = k_y$.

To calculate $L_n(z)$ we employ a transformation [13, 6, 36, 34] between radiating spherical waves and plane waves:

$$\mathrm{u}_n(k\boldsymbol{r}) = \frac{1}{2\pi\mathrm{i}^\ell}\int_{\mathbb{R}^2}\mathrm{Y}_n(\hat{\boldsymbol{q}})\mathrm{e}^{\mathrm{i}\boldsymbol{q}\cdot\boldsymbol{r}}\frac{\mathrm{d}q_x\,\mathrm{d}q_y}{kq_z}, \quad \text{for } z>0,\ \operatorname{Re}k>0,\ \operatorname{Im}k\geq 0 \tag{F.2}$$

where $\boldsymbol{q} = (q_x, q_y, q_z)$, $q_z = (k^2 - q_x^2 - q_y^2)^{1/2}$ and evaluated such that $\operatorname{Im} q_z \geq 0$. If $z<0$ we use $\mathrm{u}_n(k\boldsymbol{r}) = (-1)^\ell \mathrm{u}_n(-k\boldsymbol{r})$ and then apply the above.

Substituting the above representation into $L_n(z)$ leads to

$$L_n(z) = \begin{cases}\dfrac{1}{2\pi\mathrm{i}^\ell}\displaystyle\int_{\mathbb{R}^2}\left(\int_{\mathbb{R}^2}\mathrm{i}(k_{p_z}-q_z)\mathrm{Y}_n(\hat{\boldsymbol{q}})\mathrm{e}^{\mathrm{i}(\boldsymbol{k}_p+\boldsymbol{q})\cdot\boldsymbol{r}}\frac{\mathrm{d}q_x\,\mathrm{d}q_y}{kq_z}\right)\mathrm{d}x\,\mathrm{d}y, & z>0,\\ \dfrac{(-1)^\ell}{2\pi\mathrm{i}^\ell}\displaystyle\int_{\mathbb{R}^2}\left(\int_{\mathbb{R}^2}\mathrm{i}(k_{p_z}+q_z)\mathrm{Y}_n(\hat{\boldsymbol{q}})\mathrm{e}^{\mathrm{i}(\boldsymbol{k}_p-\boldsymbol{q})\cdot\boldsymbol{r}}\frac{\mathrm{d}q_x\,\mathrm{d}q_y}{kq_z}\right)\mathrm{d}x\,\mathrm{d}y, & z<0.\end{cases} \tag{F.3}$$

Changing the order of integration, then integrating in x and y, leads to

$$L_n(z) = \begin{cases}\dfrac{2\pi}{\mathrm{i}^\ell}\displaystyle\int_{\mathbb{R}^2}\mathrm{i}(k_{p_z}-q_z)\mathrm{Y}_n(\hat{\boldsymbol{q}})\delta(k_{p_x}+q_x)\delta(k_{p_y}+q_y)\mathrm{e}^{\mathrm{i}(k_{p_z}+q_z)z}\frac{\mathrm{d}q_x\,\mathrm{d}q_y}{kq_z}, & z>0,\\ \dfrac{2\pi}{(-\mathrm{i})^\ell}\displaystyle\int_{\mathbb{R}^2}\mathrm{i}(k_{p_z}+q_z)\mathrm{Y}_n(\hat{\boldsymbol{q}})\delta(k_{p_x}-q_x)\delta(k_{p_y}-q_y)\mathrm{e}^{\mathrm{i}(k_{p_z}-q_z)z}\frac{\mathrm{d}q_x\,\mathrm{d}q_y}{kq_z}, & z<0,\end{cases} \tag{F.4}$$

[8] After making the substitutions $T_n \to -Z_\ell$, $a_{12}\to b_{12}$, $c_{n'nn_1}\to \delta_{m_1,m'-m}4\pi(-1)^m\mathrm{i}^{\ell_1+\ell-\ell'}\mathcal{G}(\ell,m;\ell',-m';\ell_1)$, $F_{p,n}\to 4\pi\mathrm{i}^\ell Z_\ell F^m_\ell$, and $N_q(ka_{12},k_pa_{12})\to -N_q(k_pb_{12})(\mathrm{i}kb_{12})^{-1}$, followed by using $(-1)^{\ell'+\ell+\ell_1}=1$. Note that our conventions of spherical harmonics is the same theirs, and that F^m_ℓ does not depend on p as multiple effective waves was not considered in [38].

then integrating in q_x and q_y we get

$$L_n(z) = \mathrm{Y}_n(\hat{\boldsymbol{k}}_p^+)\frac{2\pi\mathrm{i}}{\mathrm{i}^\ell k q_z}\begin{cases}(-1)^m(k_{p_z}-q_z)\mathrm{e}^{\mathrm{i}(k_{p_z}+q_z)z}, & z>0,\\ (-1)^\ell(k_{p_z}+q_z)\mathrm{e}^{\mathrm{i}(k_{p_z}-q_z)z}, & z<0,\end{cases} \tag{F.5}$$

where $\boldsymbol{k}_p^+ = (k_{p_x}, k_{p_y}, q_z)$ and $q_z = (k^2 - k_{p_x}^2 - k_{p_y}^2)^{1/2}$, and we used that $\mathrm{Y}_n(\hat{\boldsymbol{k}}_p^-) = (-1)^m\mathrm{Y}_n(\hat{\boldsymbol{k}}_p^+)$ where $\boldsymbol{k}_p^- = (-k_{p_x}, -k_{p_y}, q_z)$.

In most cases where we use plane-waves, we will assume the material occupies the region $\mathcal{R}_1 = \{z > a_1 : \boldsymbol{r} \in \mathbb{R}^3\}$. In this case we have that $k_{p_x} = k_x$ and $k_{p_y} = k_y$, due to planar symmetry (3.21), which implies that $\hat{\boldsymbol{k}}_p^+ = \hat{\boldsymbol{k}}$ and $q_z = (k^2 - k_x^2 - k_y^2)^{1/2} = k_z$. Substituting these results in (F.5) then leads to

$$L_n(z) = \mathrm{Y}_n(\hat{\boldsymbol{k}})\frac{2\pi\mathrm{i}}{\mathrm{i}^\ell k k_z}\begin{cases}(-1)^m(k_{p_z}-k_z)\mathrm{e}^{\mathrm{i}(k_{p_z}+k_z)z}, & z>0,\\ (-1)^\ell(k_{p_z}+k_z)\mathrm{e}^{\mathrm{i}(k_{p_z}-k_z)z}, & z<0,\end{cases} \tag{F.6}$$

where k_{p_z} is the z component of $\boldsymbol{k}_p$. The case $z < 0$ gives the same result obtained in [38, Equation B.5].

G Proof of expansion in regular spherical waves

In this appendix, we give a simple proof of the expansion in regular spherical waves in (**??**). To this end, let $f(\boldsymbol{x})$ satisfy the Helmholtz' equation $\nabla^2 f(\boldsymbol{x}) + k_p^2 f(\boldsymbol{x}) = 0$ in a bounded region $\mathcal{R}$ where we assume Im $k_p \geq 0$.

The integral representation of the solution in $\mathcal{R}$ then is [36, Ch. 3, eqn. (3.2)]

$$\int_{\partial\mathcal{R}}\left\{g(k_p, |\boldsymbol{x}-\boldsymbol{x}_1|)\frac{\partial f(\boldsymbol{x}_1)}{\partial\nu_1} - f(\boldsymbol{x}_1)\frac{\partial g(k_p, |\boldsymbol{x}-\boldsymbol{x}_1|)}{\partial\nu_1}\right\}\mathrm{d}A_1 = \begin{cases}f(\boldsymbol{x}), & \boldsymbol{x}\in\mathcal{R}\\ 0, & \boldsymbol{x}\in\mathbb{R}^3\setminus\bar{\mathcal{R}},\end{cases} \tag{G.1}$$

where the free space Green's function is

$$g(k,r) = \frac{\mathrm{e}^{\mathrm{i}kr}}{4\pi r}.$$

The limit values of the field $f(\boldsymbol{x}_1)$ and its normal derivative are the limits from the inside of the region $\mathcal{R}$.

The Green's function has an expansion in terms of spherical waves [36, Sec. 7.5.1] and [49].

$$g(k_p, |\boldsymbol{x}-\boldsymbol{x}_1|) = \mathrm{i}k_p\sum_n \mathrm{v}_n^\dagger(k_p\boldsymbol{x}_<)\mathrm{u}_n(k_p\boldsymbol{x}_>) = \mathrm{i}k_p\sum_n \mathrm{v}_n(k_p\boldsymbol{x}_<)\mathrm{u}_n^\dagger(k_p\boldsymbol{x}_>), \tag{G.2}$$

where $\boldsymbol{x}_<$ ($\boldsymbol{x}_>$) is the position vector with the smallest (largest) distance to the origin, *i.e.*, if $x < x_1$ then $\boldsymbol{x}_< = \boldsymbol{x}$ and $\boldsymbol{x}_> = \boldsymbol{x}_1$, and the dagger symbol † denotes a complex conjugate of the spherical harmonics in the wave function. This expansion is uniformly convergent in compact (finite and closed) domains, provided $x \neq x_1$ in the domain [49, 32].

Now restrict $\boldsymbol{x}$ to lie inside the inscribed sphere of $\partial\mathcal{R}$ (we assume the origin lies inside the region $\mathcal{R}$). Insert (G.2) in (G.1), and change the order of summation and integration (legitimate due to uniform convergence of the series). We get

$$f(\boldsymbol{x}) = \sum_n a_n \mathrm{v}_n(k_p\boldsymbol{x}), \quad x < \min_{\boldsymbol{x}_1\in\partial\mathcal{R}} x_1$$

where

$$a_n = \mathrm{i}k_p\int_{\partial\mathcal{R}}\left\{\mathrm{u}_n(k_p\boldsymbol{x}_1)\frac{\partial f(\boldsymbol{x}_1)}{\partial\nu_1} - f(\boldsymbol{x}_1)\frac{\partial \mathrm{u}_n(k_p\boldsymbol{x}_1)}{\partial\nu_1}\right\}\mathrm{d}A_1.$$

References

[1] B. I. 20998-3:2017. *Measurement and characterization of particles by acoustic methods*. Vol. 3. 3 vols. London: British Standards Institution, 2017. 36 pp.

[2] G. Adomian. "The closure approximation in the hierarchy equations". en. In: *J. Stat. Phys.* 3.2 (1971), pp. 127–133.

[3] W. S. Ament. "Sound Propagation in Gross Mixtures". In: *J. Acoust. Soc. Am.* 25.4 (July 1953), pp. 638–641.

[4] J. Bezanson et al. "Julia: A fresh approach to numerical computing". In: *SIAM Review* 59.1 (2017), pp. 65–98.

[5] J. Bezanson et al. "Julia: Dynamism and Performance Reconciled by Design". In: *Proc. ACM Program. Lang.* 2.OOPSLA (Oct. 2018), 120:1–120:23.

[6] A. Boström, G. Kristensson, and S. Ström. "Transformation Properties of Plane, Spherical and Cylindrical Scalar and Vector Wave Functions". In: *Field Representations and Introduction to Scattering*. Ed. by V. V. Varadan, A. Lakhtakia, and V. K. Varadan. Acoustic, Electromagnetic and Elastic Wave Scattering. Amsterdam: Elsevier Science Publishers, 1991. Chap. 4, pp. 165–210.

[7] M. Caleap and B. W. Drinkwater. "Metamaterials: supra-classical dynamic homogenization". In: *New Journal of Physics* 17.12 (2015), p. 123022.

[8] M. Caleap, B. W. Drinkwater, and P. D. Wilcox. "Effective dynamic constitutive parameters of acoustic metamaterials with random microstructure". en. In: *New Journal of Physics* 14.3 (2012), p. 033014.

[9] R. E. Challis et al. "Ultrasound techniques for characterizing colloidal dispersions". In: *Reports on Progress in Physics* 68.7 (2005), pp. 1541–1637.

[10] M. Chekroun et al. "Comparison between a multiple scattering method and direct numerical simulations for elastic wave propagation in concrete". In: *Ultrasonic wave propagation in non homogeneous media*. Springer, 2009, pp. 317–327.

[11] M. Chekroun et al. "Time-domain numerical simulations of multiple scattering to extract elastic effective wavenumbers". en. In: *Waves in Random and Complex Media* 22.3 (2012), pp. 398–422.

[12] J.-M. Conoir and A. N. Norris. "Effective wavenumbers and reflection coefficients for an elastic medium containing random configurations of cylindrical scatterers". en. In: *Wave Motion* 47.3 (2010), pp. 183–197.

[13] M. Danos and L. C. Maximon. "Multipole Matrix Elements of the Translation Operator". In: *J. Math. Phys.* 6.5 (1965), pp. 766–778.

[14] P. J. Davis. *Interpolation & Approximation*. New York, NY: Dover Publications, 1975.

[15] A. Doicu and M. I. Mishchenko. "Electromagnetic scattering by discrete random media. I: The dispersion equation and the configuration-averaged exciting field". In: *J. Quant. Spectrosc. Radiat. Transfer* (2019).

[16] A. Doicu and M. I. Mishchenko. "Electromagnetic scattering by discrete random media. II: The coherent field". In: *Journal of Quantitative Spectroscopy and Radiative Transfer* 230 (2019), pp. 86–105.

[17] A. R. Edmonds. *Angular Momentum in Quantum Mechanics*. 3rd. Princeton, 1974.

[18] J. G. Fikioris and P. C. Waterman. "Multiple Scattering of Waves. II. "Hole Corrections" in the Scalar Case". In: *J. Math. Phys.* 5.10 (1964), pp. 1413–1420.

[19] J. G. Fikioris and P. C. Waterman. "Multiple scattering of waves. III. The electromagnetic case". In: *J. Quant. Spectrosc. Radiat. Transfer* 123 (2013), pp. 8–16.

[20] L. L. Foldy. "The multiple scattering of waves. I. General theory of isotropic scattering by randomly distributed scatterers". In: *Phys. Rev.* 67.3-4 (1945), p. 107.

[21] B. Friedman and J. Russek. "Addition theorems for spherical waves". In: *Quart. Appl. Math.* 12.1 (1954), pp. 13–23.

[22] M. Ganesh and S. C. Hawkins. "A far-field based T-matrix method for two dimensional obstacle scattering". en. In: *ANZIAM Journal* 51.0 (2010), pp. 215–230.

[23] M. Ganesh and S. C. Hawkins. "Algorithm 975: TMATROM—A T-Matrix Reduced Order Model Software". In: *ACM Trans. Math. Softw.* 44.1 (2017), 9:1–9:18.

[24] M. Ganesh, S. Hawkins, et al. "An efficient O (N) algorithm for computing O (N2) acoustic wave interactions in large N-obstacle three dimensional configurations". In: *BIT* 55 (2015), pp. 117–139.

[25] A. L. Gower, I. D. Abrahams, and W. J. Parnell. "A proof that multiple waves propagate in ensemble-averaged particulate materials". In: *Proc. R. Soc. A* 475.2229 (2019), p. 20190344.

[26] A. L. Gower, W. J. Parnell, and I. D. Abrahams. "Multiple waves propagate in random particulate materials". In: *SIAM J. Appl. Math.* 79.6 (2019), pp. 2569–2592.

[27] A. L. Gower et al. "Characterising particulate random media from near-surface backscattering: A machine learning approach to predict particle size and concentration". In: *EPL (Europhysics Letters)* 122.5 (2018), p. 54001.

[28] A. L. Gower et al. "Reflection from a multi-species material and its transmitted effective wavenumber". en. In: *Proc. R. Soc. A* 474.2212 (2018), p. 20170864.

[29] A. L. Gower. "EffectiveWaves.jl: A package to calculate ensemble averaged waves in heterogeneous materials". In: *Github github.com/JuliaWaveScattering/EffectiveWaves.jl/tree/v0.3.0* (2020).

[30] A. L. Gower and J. Deakin. "MultipleScatering.jl: A Julia library for simulating, processing, and plotting multiple scattering of waves." In: *Github github.com/JuliaWaveScattering/MultipleScattering.jl* (2020).

[31] C.-A. Guérin, P. Mallet, and A. Sentenac. "Effective-medium theory for finite-size aggregates". In: *JOSA A* 23.2 (2006), pp. 349–358.

[32] R. Kress. "Chapter 1.4.1 - Specific Theoretical Tools ". In: *Scattering*. Ed. by R. Pike and P. Sabatier. London: Academic Press, 2002, pp. 175–190.

[33] G. Kristensson. "Coherent scattering by a collection of randomly located obstacles — an alternative integral equation formulation". In: *J. Quant. Spectrosc. Radiat. Transfer* 164 (2015), pp. 97–108.

[34] G. Kristensson. *Electromagnetic scattering by a buried three-dimensional inhomogeneity in a lossy ground*. Tech. rep. Rep. 79-29. This report is also available in the author's PhD thesis on his homepage. Inst. of Theor. Phys., Göteborg, Sweden, 1979.

[35] G. Kristensson. "Evaluation of some integrals relevant to multiple scattering by randomly distributed obstacles". In: *J. Math. Anal. Appl.* 432.1 (2015), pp. 324–337.

[36] G. Kristensson. *Scattering of Electromagnetic Waves by Obstacles*. Mario Boella Series on Electromagnetism in Information and Communication. Edison, NJ, USA: SciTech Publishing, 2016.

[37] C. Kuehn. "Moment Closure—A Brief Review". en. In: *Control of Self-Organizing Nonlinear Systems*. Ed. by E. Schöll, S. H. L. Klapp, and P. Hövel. Understanding Complex Systems. Cham: Springer International Publishing, 2016, pp. 253–271.

[38] C. M. Linton and P. A. Martin. "Multiple Scattering by Multiple Spheres: A New Proof of the Lloyd–Berry Formula for the Effective Wavenumber". en. In: *SIAM J. Appl. Math.* 66.5 (2006), pp. 1649–1668.

[39] C. M. Linton and P. A. Martin. "Multiple scattering by random configurations of circular cylinders: Second-order corrections for the effective wavenumber". en. In: *J. Acoust. Soc. Am.* 117.6 (2005), p. 3413.

[40] F. Luppé, J.-M. Conoir, and A. N. Norris. "Effective wave numbers for thermo-viscoelastic media containing random configurations of spherical scatterers". In: *The Journal of the Acoustical Society of America* 131.2 (2012), pp. 1113–1120.

[41] D. W. Mackowski. "An effective medium method for calculation of the T matrix of aggregated spheres". In: *J. Quant. Spectrosc. Radiat. Transfer* 70.4-6 (2001), pp. 441–464.

[42] D. W. Mackowski and M. I. Mishchenko. "A multiple sphere T-matrix Fortran code for use on parallel computer clusters". In: *J. Quant. Spectrosc. Radiat. Transfer* 112.13 (2011), pp. 2182–2192.

[43] D. W. Mackowski and M. I. Mishchenko. "Direct simulation of multiple scattering by discrete random media illuminated by Gaussian beams". In: *Phys. Rev. A* 83.1 (2011), p. 013804.

[44] P. A. Martin. "Multiple scattering by random configurations of circular cylinders: Reflection, transmission, and effective interface conditions". In: *J. Acoust. Soc. Am.* 129.4 (2011), pp. 1685–1695.

[45] P. A. Martin. *Multiple Scattering: Interaction of Time-Harmonic Waves with N Obstacles*. en. Vol. 107. Cambridge University Press, 2006.

[46] P. A. Martin, A. Maurel, and W. J. Parnell. "Estimating the dynamic effective mass density of random composites". In: *J. Acoust. Soc. Am.* 128.2 (2010), pp. 571–577.

[47] M. I. Mishchenko, L. D. Travis, and D. W. Mackowski. "T-matrix computations of light scattering by nonspherical particles: A review". In: *J. Quant. Spectrosc. Radiat. Transfer*. Light Scattering by Non-Spherical Particles 55.5 (1996), pp. 535–575.

[48] M. I. Mishchenko et al. "First-principles modeling of electromagnetic scattering by discrete and discretely heterogeneous random media". In: *Physics Reports* 632 (2016). arXiv: 1605.06452, pp. 1–75.

[49] P. Monk. *Finite Element Methods for Maxwell's Equations*. Numerical Mathematics and Scientific Computation. Oxford: Oxford University Press, 2003.

[50] P. M. Morse and K. U. Ingard. *Theoretical acoustics*. Princeton university press, 1986.

[51] K. Muinonen et al. "Coherent Backscattering Verified Numerically for a Finite Volume of Spherical Particles". en. In: *The Astrophysical Journal* 760.2 (2012), p. 118.

[52] W. J. Parnell and I. D. Abrahams. "Multiple point scattering to determine the effective wavenumber and effective material properties of an inhomogeneous slab". en. In: *Waves in Random and Complex Media* 20.4 (2010), pp. 678–701.

[53] B. Peterson and S. Ström. "T-Matrix for Electromagnetic Scattering from an Arbitrary number of Scatterers and Representations of E(3)". In: *Phys. Rev. D* 8 (1973), pp. 3661–3678.

[54] V. J. Pinfield. "Thermo-elastic multiple scattering in random dispersions of spherical scatterers". In: *The Journal of the Acoustical Society of America* 136.6 (2014), pp. 3008–3017.

[55] V. P. Tishkovets, E. V. Petrova, and M. I. Mishchenko. "Scattering of electromagnetic waves by ensembles of particles and discrete random media". In: *J. Quant. Spectrosc. Radiat. Transfer* 112 (2011), pp. 2095–2127.

[56] L. Tsang and J. A. Kong. *Scattering of Electromagnetic Waves: Advanced Topics*. New York, NY: John Wiley & Sons, 2001.

[57] L. Tsang, J. A. Kong, and K.-H. Ding. *Scattering of Electromagnetic Waves: Theories and Applications*. New York, NY: John Wiley & Sons, 2000.

[58] L. Tsang et al. *Scattering of Electromagnetic Waves: Numerical Simulations*. New York, NY: John Wiley & Sons, 2001.

[59] V. K. Varadan. "Scattering of elastic waves by randomly distributed and oriented scatterers". en. In: *J. Acoust. Soc. Am.* 65.3 (1979), pp. 655–657.

[60] V. K. Varadan and V. V. Varadan, eds. *Low and High Frequency Asymptotics*. Vol. 2. Acoustic, Electromagnetic and Elastic Wave Scattering. Amsterdam: North-Holland, 1986.

[61] J. R. Willis. "Transmission and reflection at the boundary of a random two-component composite". In: *Proceedings of the Royal Society A* 476.2235 (2020), p. 20190811.

[62] J. R. Willis. "Transmission and reflection of waves at an interface between ordinary material and metamaterial". In: *Journal of the Mechanics and Physics of Solids* 136 (2020), p. 103678.